Supplementary Information

Efficiently healable, recyclable, and dynamically assembled high-filled energetic composites by an insulin-inspired triple dynamic network

Zhe Suna, Xiaoyan Zhanga, Shixuan Wua, Wei Jianga, Guangpu Zhanga, *

^a National Special Superfine Powder Engineering Technology Research Center, School of Chemistry and Chemical Engineering, Nanjing University of Science and Technology, Nanjing 210094, PR China.

*Corresponding Authors

E-mail: gpzhang@njust.edu.cn

Experience Section

1. Materials

The glycidyl azide polymer (GAP-diol, $M_n \sim 4000$ g/mol) was supplied from Liming Research Institute of Chemical Industry (China). The GAP-diol was heated at 90 °C under vacuum for 48 h to remove the residual moisture. The 2-Amino-4-hydroxy-6-methylpyrimidine (AHMP, 98%), hexamethylene diisocyanate (HDI, 99%), n-hexane (98%), 2-amino-2-methyl-1,3-propanediol (AMPD, 98%) were purchased from Aladdin Inc. The chloroform, diethyl ether, acetone, absolute ethyl alcohol, and ethyl acetate (analytically pure) were obtained from the National Pharmaceutical Group Chemical Reagent Co., Ltd (China). Dicyclohexylmethane 4,4'-diisocyanate (HMDI, 90%), N,N'-bis(2-hydroxyethyl)oxamide (BHO, 99%), bis(4-hydroxyphenyl) disulfide (HPS, 98%), 1-methyl-2-pyrrolidinone (NMP, 95.5%), dibutyltin dilaurate (DBTDL, 95%) were purchased from Macklin Inc. The dimethylformamide (DMF, 99.8%, Superdry) was supplied by J&K Inc. The 1,3,5-trinitro-1,3,5-trazinane (RDX, 5 μ m) and aluminum (Al, 50 nm) were produced by Yingguang Chemical Company (China). All of the solvents and reagents were used without further purification.

2. Synthesis of the UPy-diol molecule

The synthesis of UPy-diol molecule was achieved by a two-step procedure, which is showed in Figure S1. Firstly, 2-Amino-4-hydroxy-6-methylpyrimidine (80 mmol, 10.00 g) was mixed with hexamethylene diisocyanate (560 mmol, 94.20 g) under the nitrogen atmosphere. The mixture was stirred at 100 °C for 24 h with the presence of 1-methyl-2-pyrrolidinone (3 wt%). The white powder product, named as UPy-NCO, was obtained with washing with excess n-hexane and dying under vacuum overnight. The ¹H NMR spectrum of UPy-NCO was displayed in Figure S2. Secondly, the UPy-NCO molecule (10 mmol, 2.93 g) was mixed with 2-amino-2-methyl-1,3-propanediol (14 mmol, 1.47 g) in a round bottom flask. The mixture was stirred in the dried chloroform solution at 60 °C for 5 h under the protection of nitrogen atmosphere. After reaction, the crude product was acquired by the washing with excess chloroform solution. Then, this dried crude product was dissolved in dimethylformamide to obtain the cloudy solution, and a supernatant liquid was obtained by the high-speed centrifugation. Finally, the UPy-diol molecule was obtained by precipitation in diethyl ether, washing with acetone, and vacuum drying process. The ¹H NMR spectrum of UPy-diol molecule was presented in Figure S3, demonstrating the successful completing of the reaction.

3. Synthesis of the self-healing energetic polymers

A two-step polycondensation procedure was employed for generating the self-healing

energetic polymers (MHNPU-1-5). The reaction route and feed ratios of MHNPU polymers are presented in Figure S4 and Table S1. The following is an example of the preparation procedure for MHNPU-2. In the first step, GAP-diol (1 mmol, 4.1917 g) was added to a three-neck flask and vacuum degassed at 110 °C for 2 h. Then, the system was cooled to 80 °C and equipped with nitrogen atmosphere. In the second step, the HMDI (2.10 mmol, 0.5509 g), dissolved in the anhydrous DMF solution (5 mL), was added into the system with a mechanical agitation for 30 min. Subsequently, this system polymerized at 80 °C for 4 h with the assistance of dibutyltin dilaurate (0.1 wt%). In the third step, mixed chain extenders, including HPS (0.4 mmol, 0.1001 g), HBO (0.45 mmol, 0.0792 g), and UPy-diol (0.15 mmol, 0.0598 g), were further added into the flask. The chain propagation reaction was performed at a temperature of 60 °C for another 24 hours. Finally, the mixture was poured into polytetrafluoroethylene (PTFE) mold for drying at 80 °C for 48 hours in an air oven. The polymer film of MHNPU-2 was obtained after the vacuum drying procedure at a temperature of 75 °C for 24 hours.

4. Preparation of the high-filled energetic composites

The 1,3,5-trinitro-1,3,5-trazinane (RDX, used as high-energy oxidizer) and aluminum powders (Al, used as metal fuel) were selected to be solid fillers for energetic composites. The composites are identified as DSP-1-3 based on the different formulations. The mass fractions of RDX, Al, and MHNPU-2 in DSP-1 were 70%, 10%, and 20 wt%, in DSP-2 were 60%, 20%, and 20 wt%, and in DSP-3 were 50%, 30%, and 20 wt%, respectively. The preparation of the dynamic energetic composites was achieved by the shear calendaring process. An example of a DSP-1 preparation process is shown below. Firstly, the MHNPU-2 (2 g), dissolved in ethyl acetate, mixed with RDX (7 g) and Al powder (1 g) in the beaker. After solvent evaporation, the viscous composites mixture was obtained with a continuous stirring. Consequently, the mixture was dried in a fume hood at 60 °C for 24 hours, and placed in a vacuum fume for another 12 hours. Finally, this mixture was mixed uniformly using a double-roll machine at a temperature of 60 °C, which provided the longitudinal pressure and shear force. The energetic composites films were subjected to hot-pressing process at a temperature of 60 °C and a compression pressure of 5 MPa. Hydroxyl-terminated polybutadiene, a non-energetic binder, was employed to generate an energetic composite by the same method, designated HSP-3. The mass fractions of RDX and Al in HSP-3 were 50% and 30%, respectively.

5. Dynamic assembly of the energetic composites

The dynamic assembly of diverse energetic composites were achieved by the homogeneous and heterogeneous assembly. Primarily, the energetic composites films were positioned in oven at

60 °C for 1 minute to initiate the dynamics. Then, the smooth interface of two films were fitted together. The dynamic assemblies of energetic composites were achieved after continuous heating for a duration of 48 hours. These samples were named as DSP-1-1, DSP-1-2, DSP-1-3, DSP-2-2, DSP-2-3, and DSP-3-3, respectively. For instance, DSP-1-2 indicated the dynamic assembled sample of DSP-1 and DSP-2.

6. Characterization

General Characterization

The nuclear magnetic resonance spectrometer (¹H NMR) were recorded on a Bruker AVANCE III 500 MHz NMR spectrometer using CDCl₃ and DMSO-d₆ as solvent. Fourier transform infrared spectroscopy (FT-IR spectra) were recorded using a Bruker Tensor II spectrometer equipped with an attenuated total reflectance (ATR) accessory. The molecular weight of polymers was determined by gel permeation chromatography (GPC) instrument (Waters 1515), which used DMF as the mobile phase. X-ray diffraction (XRD) analysis was carried out using an X-ray diffractometer (Bruker D8 Advance), which is equipped with a Cu Kα source and works in the 2θ range of 5-60 at 40 kV and 40 mA. X-ray photoelectron spectroscopy (XPS) was carried out on Thermo Scientific K-Alpha. TGA measurement was performed on Mettler 851e instrument with a heating rate of 10 K/min from 50 to 600 °C under nitrogen atmosphere. DSC experiments were performed on a TA instrument DSC-25 at the heating rates of 5,10,15, and 20 K/min under nitrogen atmosphere. The microphase separation was observed using atomic force microscope technology (AFM, Bruker Multimode 8) with the tapping mode. The morphologies of the energetic composites were tested using scanning electron microscopy (SEM, Hitachi SU8100). The element contents were measured by an organic element analyzer (EA, Elementar Vario EL). The heat of combustion and explosion were recorded by a Parr 6200 Calorimeter with an oxygen and nitrogen atmosphere. The combustion process was recorded by a high-speed camera (Phantom VEO-E 310) with a homemade ignition device. Besides, the gaseous products of MHNPU-2 were examined using the combined characterization technique of TG-FTIR-MS, which comprised a thermogravimetric analyzer (Mettler TGA/DSC1), an FTIR spectrophotometer (Nicolet IS 10), and a mass spectrometer (Thermostar GAS analysis system). Specifically, the polymer underwent heating in an argon atmosphere from 300 to 900 K at a heating rate of 10 K/min. Then, the produced gaseous products were conveyed by the carrier gas to the cell of an FTIR spectrometer a mass spectrometry instrument. The experiment wavenumber range for FTIR was 4000 to 400 cm⁻¹, and the mass range for MS was 10 to 200.

Mechanical and self-healing experiments

Mechanical tensile tests were performed on a Reger RGM-6001 tester with a 100 N sensor at room temperature. The deformation rates were 100 and 10 mm/min for the polymers and energetic composites, respectively. The rheological measurements were performed on a TA DHR-1 rheometer with a 20-mm parallel steel plate. Frequency sweeps were performed at a rotational strain amplitude of 0.1% by varying the frequency from 100 to 0.01 Hz. Temperature sweeps were increased from 25 to 125 °C with a frequency of 1 Hz and a heating rate of 5 K/min. Optical microscopy images of the scratch self-healing process were recorded by Olympus (BX53) optical microscope. To further evaluate the self-healing ability, sample films were completely cut in half at room temperature. Then, the two pieces of the specimens were manually merged and healed under different condition. The healing efficiency is quantified as the ratio of the mechanical parameters (such as stress, strain, and toughness) of the healed sample to those of the original sample.

Molecular dynamics simulation

The molecular dynamics simulations of polymers and energetic composites were executed with Materials Studio 2019 software. The simulations of polymers were based on the condensedphase optimized molecular potential for the atomistic simulation studies II (COMPASS II) force field. The simulations of energetic composites were also based on the COMPASS II force field. Primarily, the polymer chain's molecular models, which comprises GAP, HMDI, HPS, HDO, and UPy units, were constructed and optimized. After that, the amorphous cell of MHNPU-1-5 consisting eight polymer chains were constructed by setting an initial density of 1.0 g/cm³. The smart algorithm was selected to perform the geometry optimization process until convergence. Subsequently, the model was subjected to 500 ps of the NPT ensemble at one bar pressure and then 500 ps of an NVT ensemble to obtain the final micro-information. The Andersen barostat and Nose thermostat were used to control pressure and temperature, respectively. For the crack model, it consisted of three layers structure. The first and third layers are the optimized amorphous cells of MHNPU-2, and the second layer is vacuum layer acted as the microcrack. The crack model was subjected to 500 ps of NVT ensemble at 25 °C to simulate the self-healing process in real life. The electrostatic interactions were calculated using the Ewald summation method and the van der Waals interactions were calculated using the Lennard-Jones function. The cutoff distance of non-bonded interactions composed of electrostatic and van der Waals components is 12.5 Å.

The variation tendency in energy and hydrogen bonds during kinetic simulation were acquired via script file. The binding energy of hard domain and the interfacial binding energy were obtained from the equilibrium as follow:

$$E_{bind} = - E_{int} = - \left(E_{AB} - E_A - E_B \right)$$

Where E_{AB} represents the single point energy of A and B entirety, E_{A} and E_{B} represents the single point energy of A and B counterpart, respectively. When the value of E_{bind} exceed zero, it suggest that an attraction force between A and B, and the opposite indicated the existence of repulsive force.

Using the aforementioned method, an optimized amorphous structure model with four polymer molecular weights was obtained. Following that, the LAMMPS software was utilized to construct the structural optimization and reactive molecular dynamics simulation of the MHNPU-2 polymer pyrolysis reaction by the ReaxFF force field. The structural optimization was performed in constant volume mode to acquire the converged molecular configuration. The reactive molecular dynamics simulation was conducted at 3000 K for a duration of 5 ps. In this term, the remaining parameters of this simulation are as follows: The time step was 0.25 fs, the equilibration duration was 1 ps, the production duration was 10 ps, and the ensemble was NVT. The pyrolysis products were ultimately evaluated using script-based statistical techniques.

Figure S1 The synthetic route of (a) UPy-NCO molecule and (b) UPy-diol molecule.

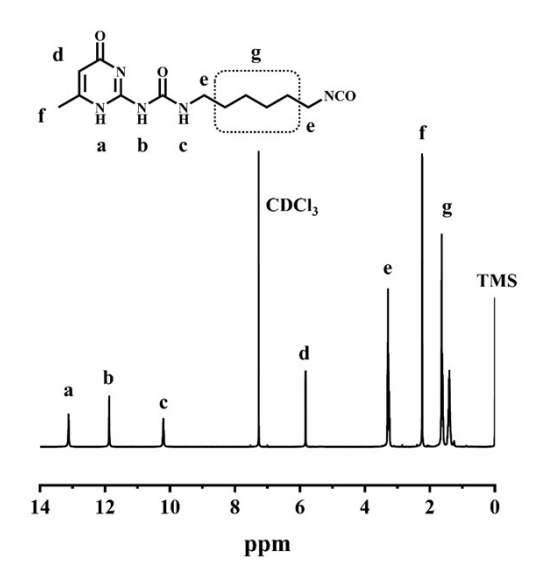


Figure S2 ^1H NMR spectrum of UPy-NCO molecule with CDCl3 as the solvent.

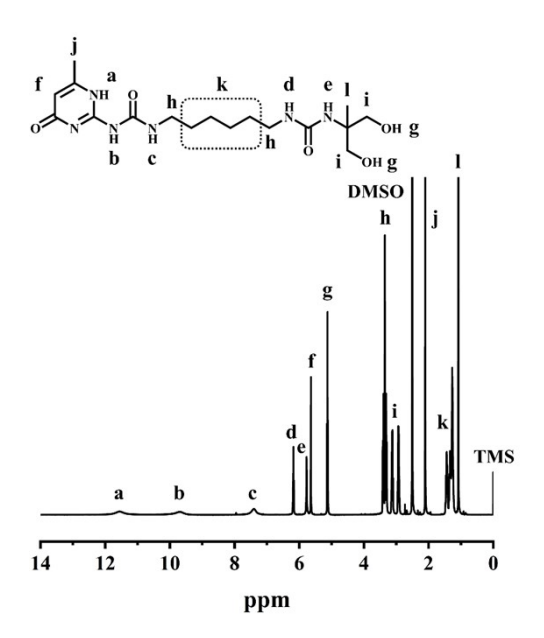


Figure S3 ^1H NMR spectrum of UPy-diol molecule with DMSO-d6 as the solvent.

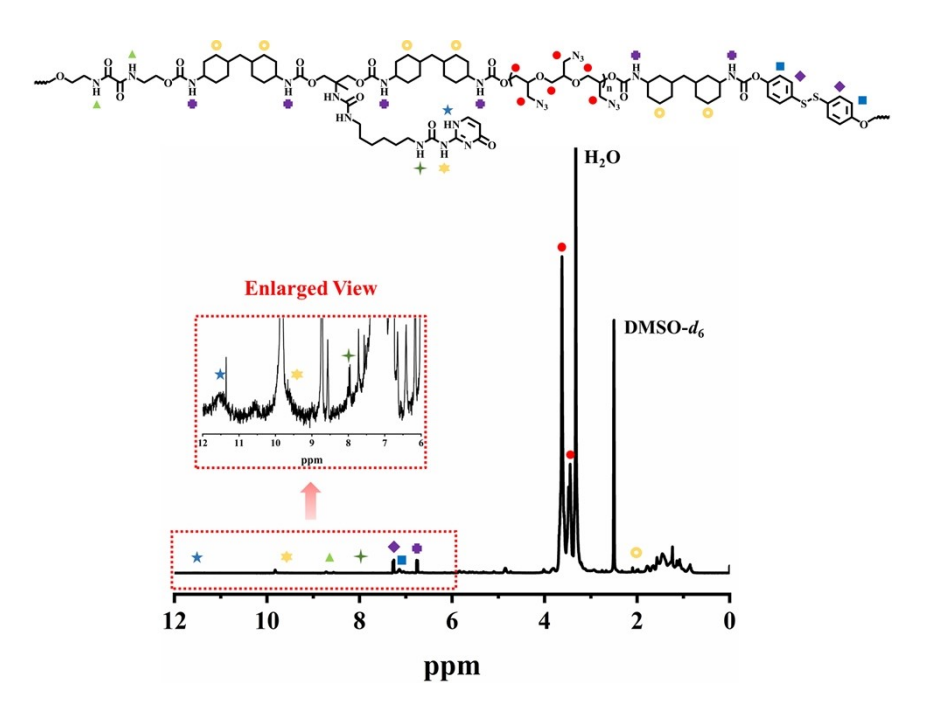


Figure S4 1 H NMR spectrum of MHNPU-2 polymer with DMSO-d₆ as the solvent.

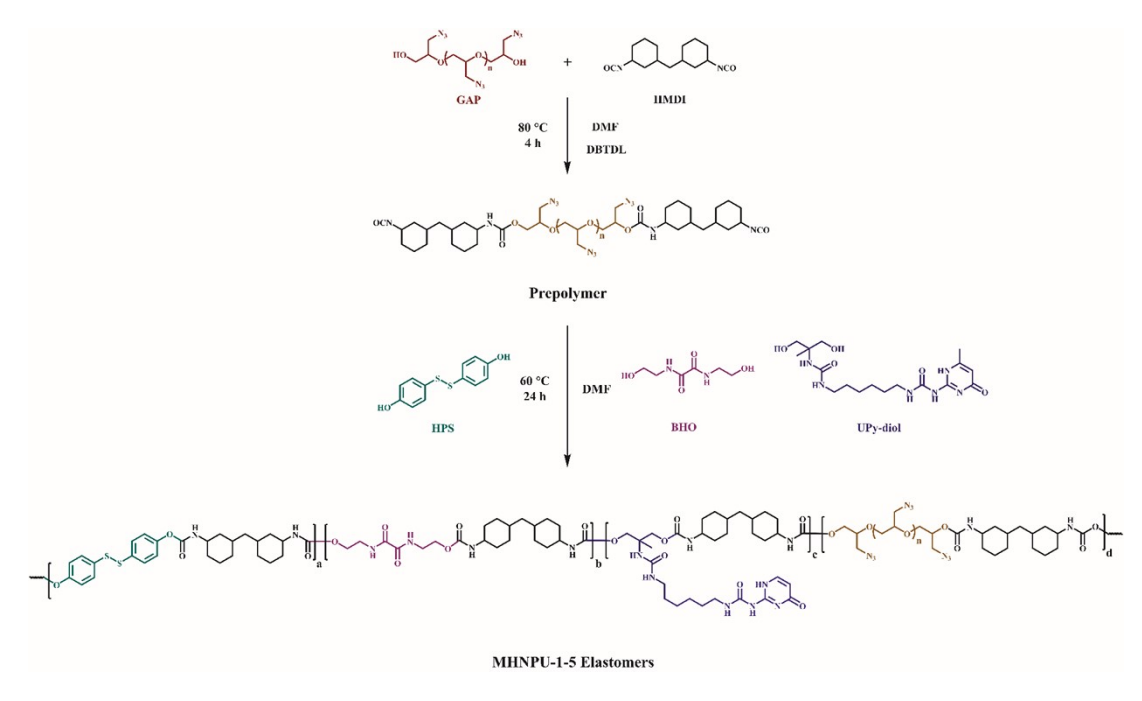


Figure S5 The synthetic route of MHNPU-1-5 elastomers via a two-step polycondensation.

Table S1 The chemical formula of MHNPU -1-5 elastomers.

Sample	GAP-diol (mmol)	HMDI (mmol)	HPS (mmol)	BHO (mmol)	UPy-diol (mmol)	HS (%)
MHNPU-1	1.00	2.10	0.40	0.60	0.00	15.91
MHNPU-2	1.00	2.10	0.40	0.45	0.15	16.49
MHNPU-3	1.00	2.10	0.40	0.30	0.30	17.07
MHNPU-4	1.00	2.10	0.40	0.15	0.45	17.64
MHNPU-5	1.00	2.10	0.40	0.00	0.60	18.20

Table S2 The molecular weight of MHNPU-1-5 elastomers.

Sample	M _n (g/mol)	M _w (g/mol)	PDI
MHNPU -1	37616	89338	2.375
MHNPU -2	32973	74244	2.252
MHNPU -3	40048	83874	2.094
MHNPU -4	31090	69740	2.243
MHNPU -5	31001	72539	2.339

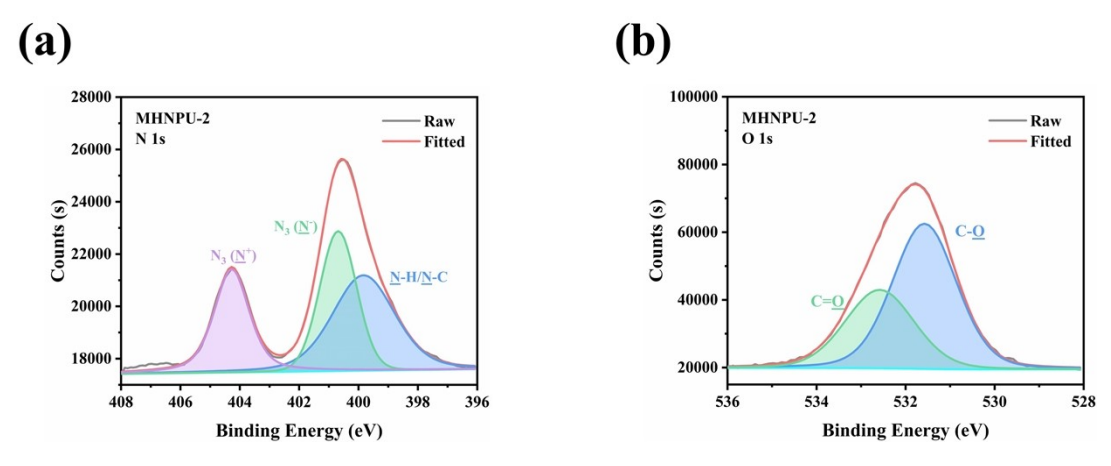


Figure S6 (a) The high-resolution N 1s XPS spectra of MHNPU-2. (b) The high-resolution O 1s XPS spectra of MHNPU-2.

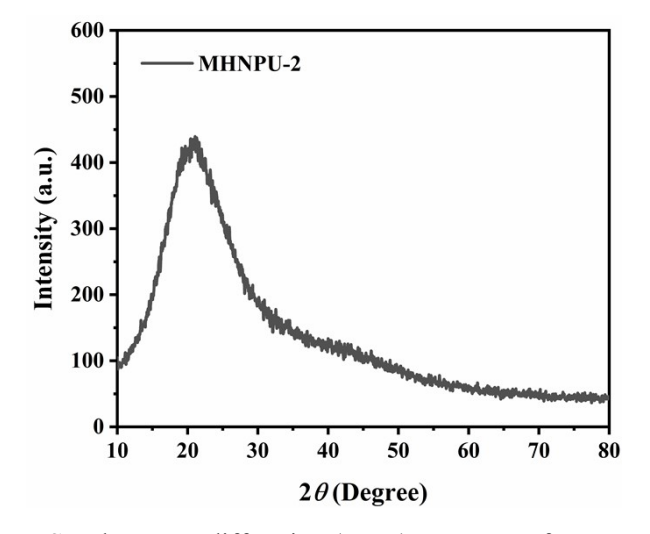


Figure S7 The X-ray diffraction (XRD) spectrum of MHNPU-2.

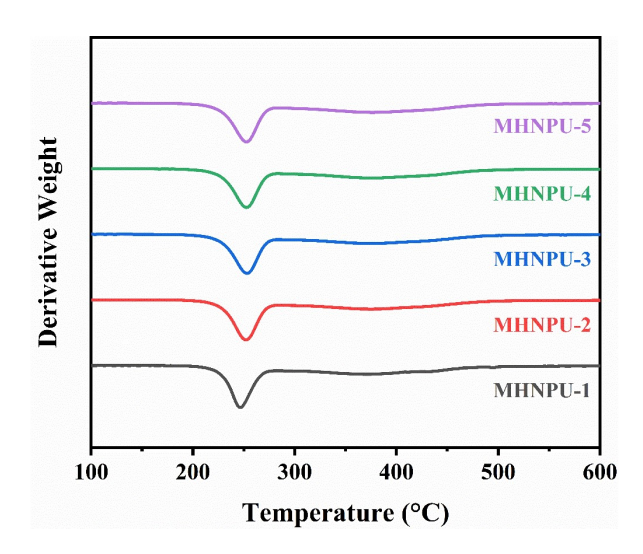


Figure S8 The derivative thermogravimetric curves of MHNPU-1-5 elastomers.

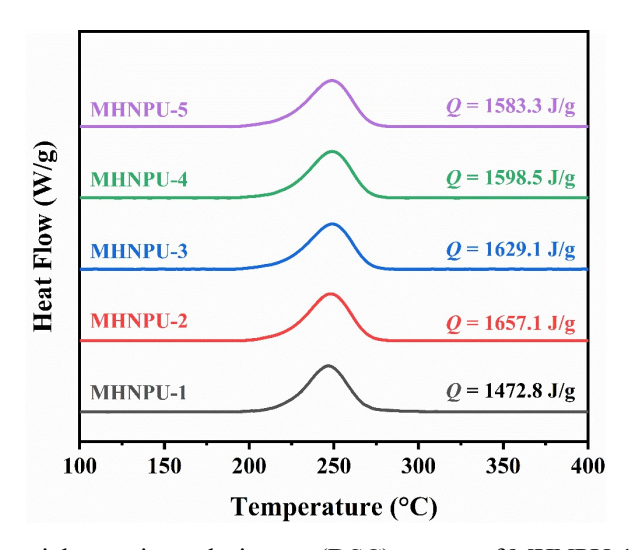


Figure S9 The differential scanning calorimetry (DSC) curves of MHNPU-1-5 elastomers with a heating rate of 10 K/min.

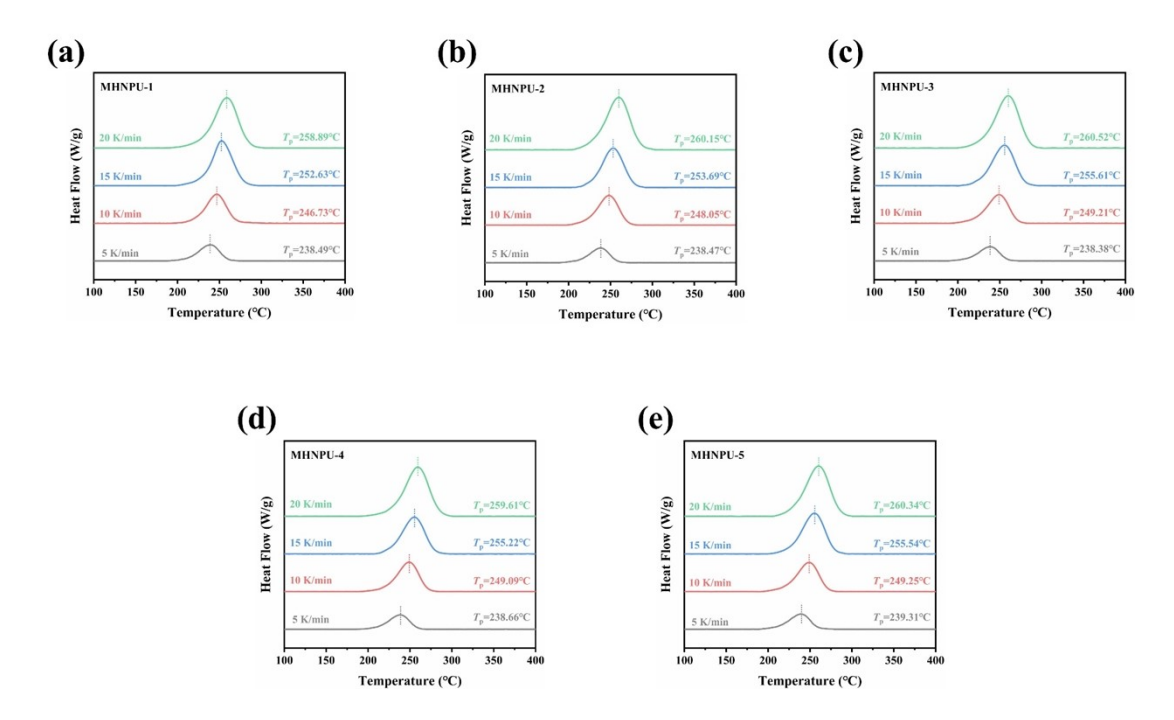


Figure S10 The differential scanning calorimetry (DSC) curves of (a) MHNPU-1, (b) MHNPU-2, (c) MHNPU-3, (d) MHNPU-4, and (e) MHNPU-5 with different heating rates (5, 10, 15, and 20 K/min).

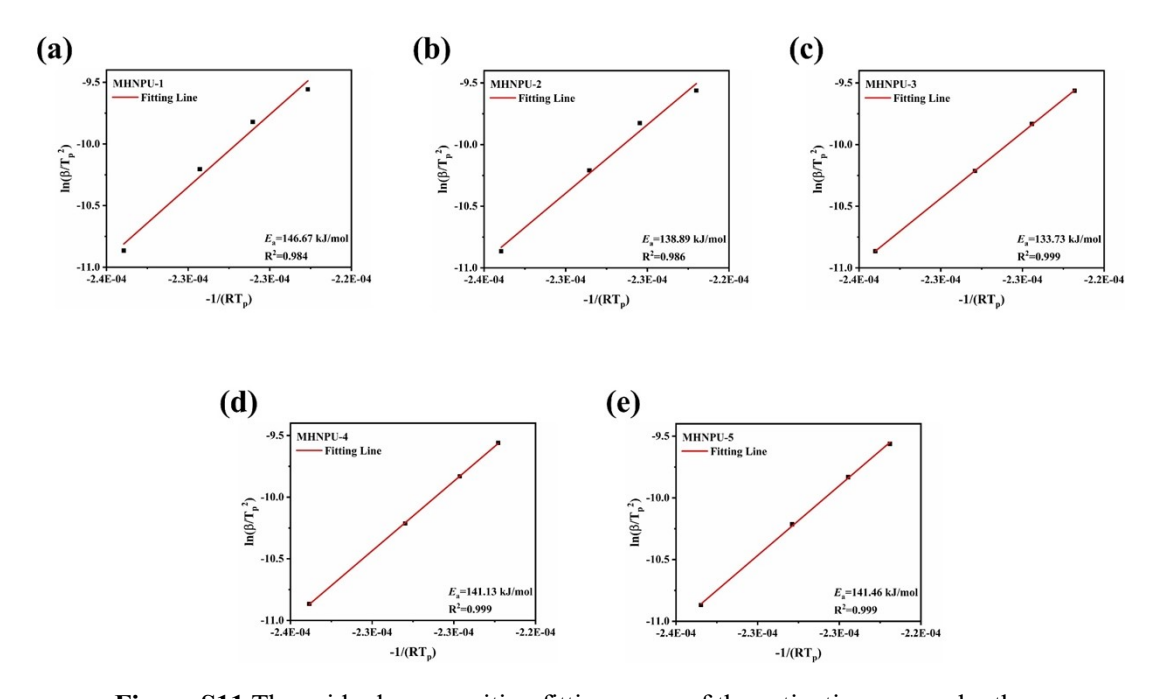


Figure S11 The azido decomposition fitting curve of the activation energy by the Kissinger equation for (a) MHNPU-1, (b) MHNPU-2, (c) MHNPU-3, (d) MHNPU-4, and (e) MHNPU-5.

Table S3 The kinetic, thermodynamic and thermal stability parameters of MHNPU elastomers.

Comple	In A	T_b	T_{SADT}	ΔS [≠]	ΔH [≠]	ΔG^{\neq}
Sample	lnA	(°C)	(°C)	(J mol ⁻¹ K ⁻¹)	(kJ mol ⁻¹)	(kJ mol ⁻¹)
MHNPU-1	26.55	239.10	224.17	+5.61	+142.53	+139.74
MHNPU -2	24.64	234.69	219.19	-10.16	+134.78	+139.80
MHNPU -3	23.37	235.32	219.18	-20.77	+129.63	+139.87
MHNPU -4	25.14	235.68	220.37	-6.07	+137.01	+140.02
MHNPU -5	25.19	237.97	222.56	-5.70	+137.33	+140.16

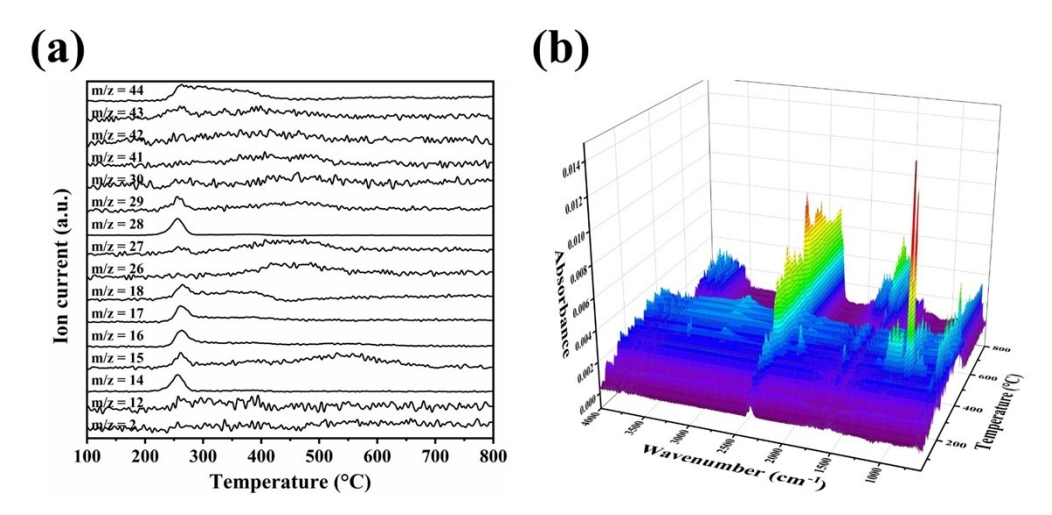


Figure S12 (a) MS curves and (b) 3D TG/FTIR spectra of gas products during the pyrolysis process of MHNPU-2.

Table S4 Peak temperature and most probable chemical structure of the FTIR and MS methods during the pyrolysis of MHNPU-2.

Stage	Method	Most possible chemical structure
	FTIR	N-H (3332, v), CO ₂ (2362, v), N ₂ (2105, v), NO ₂ (1626, v), HCN (963,
First	(cm ⁻¹)	ν).
	MS	H ₂ (2); C (12); N (14); CH ₃ ⁺ (15); NH ₂ (16); NH ₃ OH (17); H ₂ O, NH ₄ ⁺
step		(18); HCN (27); N ₂ (28); C ₂ H ₅ ⁺ , CHO (29); NO (30); N ₃ ⁺ (42); C ₃ H ₇ ⁺ ,
	(m/z)	C ₂ H ₃ O (43); N ₂ O, CO ₂ (44).
	FTIR	-OH (>3600, v), -CH ₃ /-CH ₂ (2931, v), CO ₂ (2362, v), C=O (1726, v),
Casand	(cm ⁻¹)	C=C (1503, v), HCN (968, v).
	Second	H ₂ (2); C (12); CH ₃ ⁺ (15); H ₂ O (18), CN ⁺ , C ₂ H ₂ (26); HCN (27); C ₂ H ₅ ⁺ ,
step	MS	CHO (29); HCHO (30); C ₂ H ₃ N (41); C ₂ H ₂ O (42); C ₃ H ₇ ⁺ , C ₂ H ₃ O (43);
	(m/z)	C ₂ H ₄ O, CO ₂ (44).

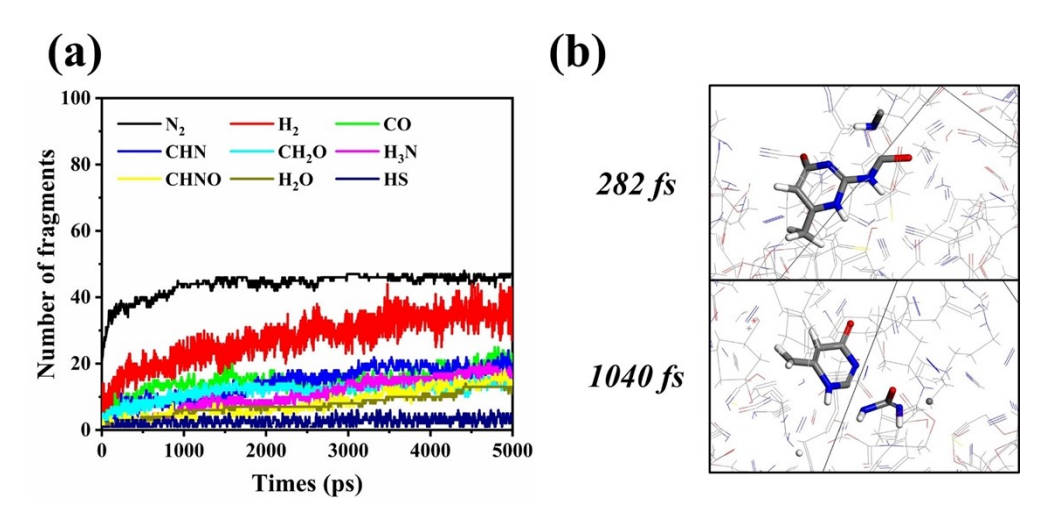


Figure S13 (a) Time evolution of typical species for MHNPU-2 model pyrolysis at 3000 K; (b) The pyrolysis process of UPy groups in above molecular simulation.

Table S5. Element composition and assumed chemical formula of MHNPU-1-5 by element analyzer.

Sample	C (%)	H (%)	O (%)	N (%)	S (%)	Assumed chemical formula
MHNPU-1	41.52	5.60	15.95	36.38	0.55	$C_{3.54}H_{5.60}O_{1.99}N_{2.30}S_{0.03}$
MHNPU-2	40.98	5.39	16.96	36.10	0.57	$C_{3.42}H_{5.39}O_{2.12}N_{2.58}S_{0.04}$
MHNPU-3	41.11	5.41	16.90	36.02	0.56	$C_{3.43}H_{5.41}O_{2.11}N_{2.57}S_{0.04}$
MHNPU-4	41.41	5.41	16.80	35.78	0.60	$C_{3.45}H_{5.41}O_{2.10}N_{2.56}S_{0.04}$
MHNPU-5	41.58	5.60	16.13	36.18	0.51	$C_{3.46}H_{5.60}O_{2.02}N_{2.58}S_{0.03}$

Table S6 A comparison of the heat of combustion and enthalpies of formation of our MHNPU polymer with those of other documented energetic polymers.

Sample	$\Delta_{\rm c}H^0({\rm kJ/g})$	$\Delta_{\rm f}H^0({\rm kJ/g})$	Ref.
ETPU 900	-22.30	-0.50	49
ETPE 1300	-21.50	-0.21	49
ETPU 2900	-21.70	+0.67	49
ETPU PolyNIMMO	-21.50	-2.29	49
ETPU PolyGLYN	-16.50	-2.07	49
P(BAMO/AMMO) ETPU	/	+3.75	50
GSPU2.5	-21.83	+0.21	51
AAE-3	-21.95	+0.04	25

Table S7 The summary of the mechanical propertis of MHNPU-1-5 elastomers.

Sample	Maximum tensile strength (MPa)	Elongation at break (%)	Toughness (MJ m ⁻³)	Young's modulus (MPa)
MHNPU-1	0.35±0.03	2271±43	6.14±0.23	0.18±0.02
MHNPU-2	0.57±0.02	2203±57	9.76±0.31	0.35±0.04
MHNPU-3	0.61±0.05	1930±39	9.29 ± 0.27	0.29±0.03
MHNPU-4	0.91±0.07	1709±51	12.52±0.33	0.48 ± 0.05
MHNPU-5	1.28±0.17	1448±46	14.58±0.49	0.59 ± 0.07

Figure S14 True stress-strain curves of MHNPU-1-5 elastomers.

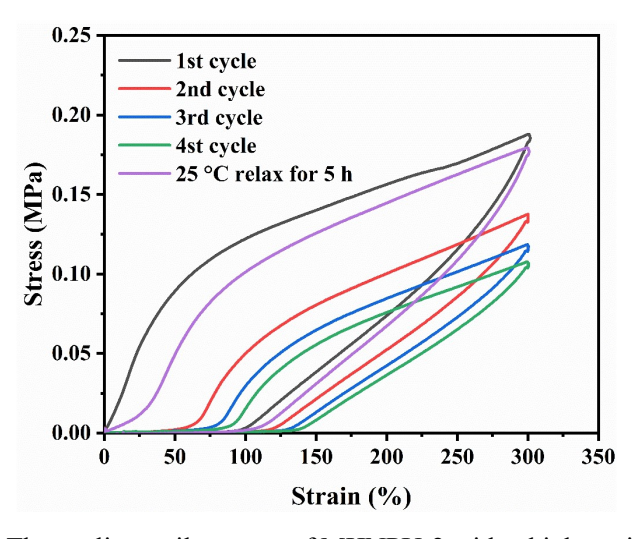


Figure S15 The cyclic tensile curves of MHNPU-2 with a high strain of 300 %.

Quantum Chemical Calculations

The investigation employed density functional theory (DFT) within the Gaussian09 software to perform quantum chemical calculations. The structural optimization and frequency calculation were conducted at the b3lyp/6-31G level. The optimized molecular structures were displayed using the UCSF Chimera 1.16 software. The azido-azido dipole interaction, hydrogen bond, and disulfide bond energies were calculated via the following equation.

$$E_{bind} = -E_{int} = -(E_{AB} - E_A - E_B)$$

Where E_{AB} represents the single-point energy of the A and B assemblies, E_{A} and E_{B} respectively denote the single-point energy of the A and B counterparts.

1) The azido-azido dipole interaction

The structure of azido unit is as shown:



Figure S16 Optimized structure of azido unit.

The energy of azido unit is:

The total electronic energy = -204.006592 Hartree

Thermal correction to Energy = 0.054439 Hartree

 $E_{\rm A}$ = ϵ_0 + $E_{\rm tot}$ =Sum of electronic and thermal energies = -203.952153 Hartree = -127982.0155 kcal/mol

The structure of azido-azido is shown as below:

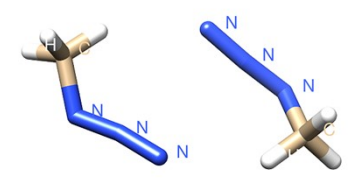


Figure S17 Optimized structure of azido-azido.

The energy of azido-azido is:

The total electronic energy = -408.018585 Hartree

Thermal correction to Energy = 0.112123 Hartree

 $E_{\rm A}$ == ε_0 + $E_{\rm tot}$ = Sum of electronic and thermal energies = -407.906462 Hartree = -255965.3840 kcal/mol

The energy of azido-azido dipole interaction:

$$\Delta E_{\text{dip}} = E_{AB} - E_{A} - E_{B} = -1.35 \text{ kcal/mol}$$

2) The hydrogen bond interactions

The structure of **carbamate** is as shown:

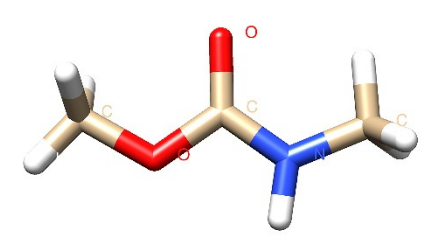


Figure S18 Optimized structure of carmabate unit.

The energy of carbamate is:

The total electronic energy = -323.643552 Hartree

Thermal correction to Energy = 0.115559 Hartree

 $E_{\rm A}$ = ϵ_0 + $E_{\rm tot}$ =Sum of electronic and thermal energies = -323.527993 Hartree = -203017.0509 kcal/mol

The structure of **urea** is as shown:

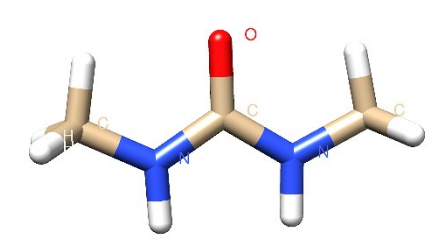


Figure S19 Optimized structure of urea unit.

The energy of urea is:

The total electronic energy = -303.788448 Hartree

Thermal correction to Energy = 0.128482 Hartree

 $E_{\rm A}$ = ϵ_0 + $E_{\rm tot}$ =Sum of electronic and thermal energies = -303.659966 Hartree = -190549.6653 kcal/mol

The structure of **BHO unit** is as shown:

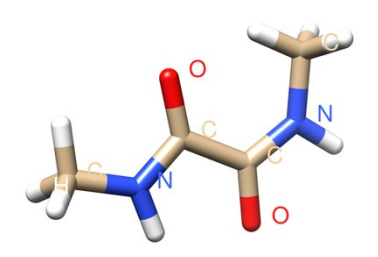


Figure \$20 Optimized structure of BHO unit.

The energy of **BHO unit** is:

The total electronic energy = -417.089089 Hartree

Thermal correction to Energy = 0.140902 Hartree

 $E_{\rm A}$ = ϵ_0 + $E_{\rm tot}$ =Sum of electronic and thermal energies = -416.948187 Hartree = -261638.9067 kcal/mol

The structure of **UPy unit** is as shown:



Figure S21 Optimized structure of UPy unit.

The energy of **UPy unit** is:

The total electronic energy = -835.1526982 Hartree

Thermal correction to Energy = 0.290934 Hartree

 $E_{\rm A}$ = ϵ_0 + $E_{\rm tot}$ =Sum of electronic and thermal energies = -834.861765 Hartree = - 523884.1062 kcal/mol

The structure of **azido-carbamate** is as shown:

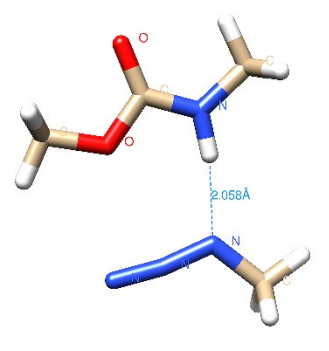


Figure S22 Optimized structure of azido-carbamate.

The energy of azido-carbamate is:

The total electronic energy = -527.658606 Hartree

Thermal correction to Energy = 0.173058 Hartree

 $E_{\rm A}$ = ϵ_0 + $E_{\rm tot}$ =Sum of electronic and thermal energies = -527.485548 Hartree = -331002.4562

kcal/mol

The energy of H bonds for azido-carbamate:

$$\Delta E_{\rm H} = E_{\rm AB} - E_{\rm A} - E_{\rm B} = -3.39 \text{ kcal/mol}$$

The structure of azido-urea is as shown:

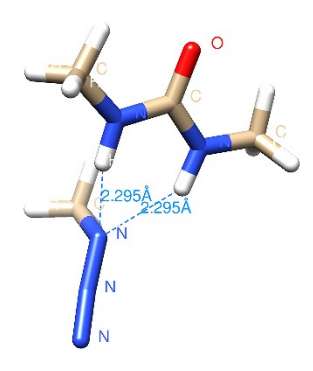


Figure S23 Optimized structure of azido-urea.

The energy of azido- urea is:

The total electronic energy = -507.805872 Hartree

Thermal correction to Energy = 0.186358 Hartree

 $E_{\rm A}$ = ϵ_0 + $E_{\rm tot}$ =Sum of electronic and thermal energies = -507.619514 Hartree = -318536.3212 kcal/mol

The energy of H bonds for azido-urea:

$$\Delta E_{\rm H} = E_{\rm AB} - E_{\rm A} - E_{\rm B} = -4.64 \text{ kcal/mol}$$

The structure of **carbamate-carbamate** is as shown:

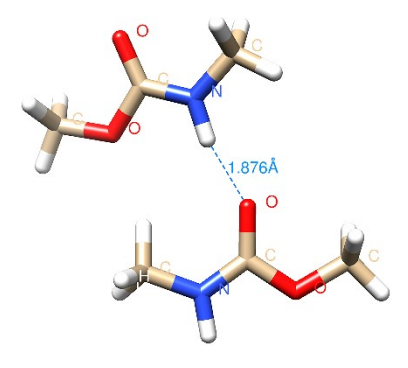


Figure S24 Optimized structure of carbamate-carbamate.

The energy of carbamate-carbamate is:

The total electronic energy = -647.301489 Hartree

Thermal correction to Energy = 0.234387 Hartree

 $E_{\rm A}$ = ϵ_0 + $E_{\rm tot}$ =Sum of electronic and thermal energies = -647.067102 Hartree = -406041.0772 kcal/mol

The energy of H bonds for carbamate-carbamate:

 $\Delta E_{\rm H} = E_{\rm AB} - E_{\rm A} - E_{\rm B} = -6.98 \text{ kcal/mol}$

The structure of **carbamate-urea** is as shown:

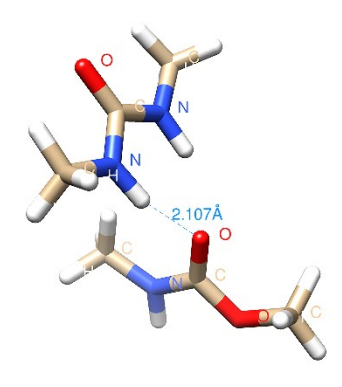


Figure S25 Optimized structure of carbamate-urea.

The energy of carbamate - urea is:

The total electronic energy = -627.4494412 Hartree

Thermal correction to Energy = 0.247739 Hartree

 $E_{\rm A}$ = ϵ_0 + $E_{\rm tot}$ =Sum of electronic and thermal energies = -627.201703 Hartree = -393575.3407 kcal/mol

The energy of H bonds for carbamate - urea:

 $\Delta E_{\rm H} = E_{\rm AB} - E_{\rm A} - E_{\rm B} = -8.35 \text{ kcal/mol}$

The structure of **urea- urea** is as shown:

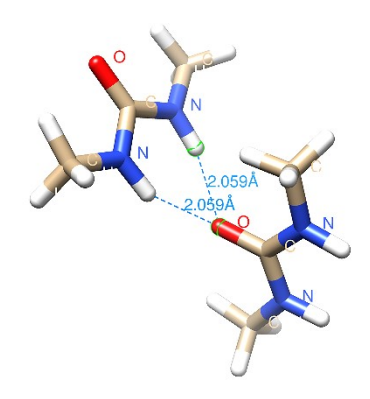


Figure S26 Optimized structure of urea-urea.

The energy of urea- urea is:

The total electronic energy =-607.597173 Hartree

Thermal correction to Energy = 0.260828 Hartree

 $E_{\rm A}$ = ϵ_0 + $E_{\rm tot}$ =Sum of electronic and thermal energies = -607.336345 Hartree = -381109.6299 kcal/mol

The energy of H bonds for urea- urea:

 $\Delta E_{\rm H} = E_{\rm AB} - E_{\rm A} - E_{\rm B} = -10.30 \text{ kcal/mol}$

The structure of **BHO-BHO** is as shown:

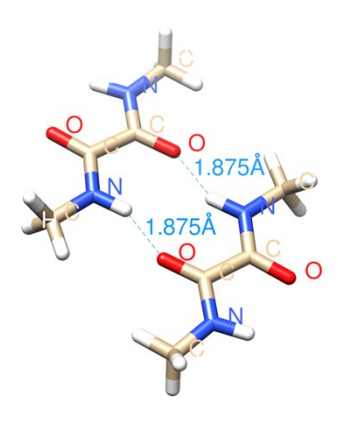


Figure S27 Optimized structure of BHO-BHO unit.

The energy of **BHO-BHO** is:

The total electronic energy = -834.221602 Hartree

Thermal correction to Energy = 0.285273 Hartree

 $E_A = \varepsilon_0 + E_{tot} = \text{Sum of electronic and thermal energies} = -833.936329 \text{ Hartree} = -523302.885449$

kcal/mol

The binding energy of H-bonds for BHO-BHO:

 $\Delta E_{\rm H} = E_{\rm AB} - E_{\rm A} - E_{\rm B} = -25.07 \text{ kcal/mol}$

The structure of **UPy- UPy** is as shown:



Figure S28 Optimized structure of UPy-UPy.

The energy of UPy- UPy is:

The total electronic energy = -1670.3948918 Hartree

Thermal correction to Energy = 0.587006 Hartree

 $E_A = \varepsilon_0 + E_{tot} = \text{Sum of electronic and thermal energies} = -1669.807886 \text{ Hartree} = -1047821.1465 \text{ kcal/mol}$

The energy of H bonds:

 $\Delta E_{\rm H} = E_{\rm AB} - E_{\rm A} - E_{\rm B} = -52.93 \text{ kcal/mol}$

3) The disulfide bond interaction

The structure of **HPS unit (one half)** is as shown:

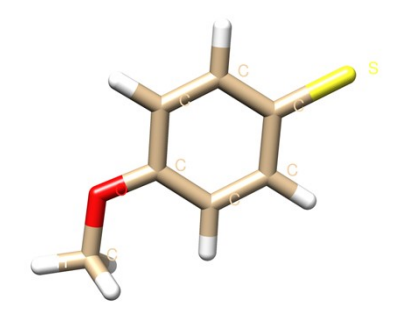


Figure S29 Optimized structure of HPS unit (one half).

The energy of HPS unit (one half) is:

The total electronic energy = -744.225785 Hartree

Thermal correction to Energy = 0.132445 Hartree

 $E_A = \varepsilon_0 + E_{tot} = \text{Sum of electronic}$ and thermal energies = -744.093340 Hartree = -466925.565327 kcal/mol

The structure of **HPS unit** is as shown:

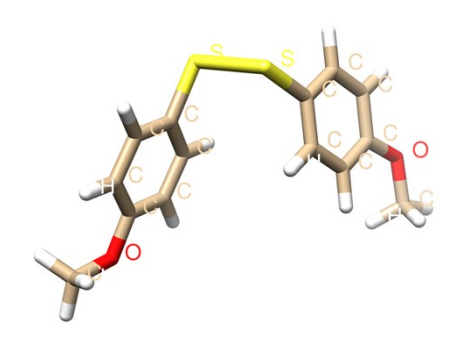


Figure S30 Optimized structure of HPS unit.

The energy of **HPS unit** is:

The total electronic energy = -1488.488695 Hartree

Thermal correction to Energy = 0.268427 Hartree

 $E_{\rm A}=\epsilon_0+E_{\rm tot}$ =Sum of electronic and thermal energies = -1488.220268 Hartree = -933872.207440 kcal/mol

The binding energy of disulfide bond:

 $\Delta E_{\text{disulfide}} = E_{AB} - E_{A} - E_{B} = -21.08 \text{ kcal/mol}$

Table S8 The summary of the binding energies for azido-azido dipole interaction, hydrogen bonds, and disulfide bond in the MHNPU elastomers.

Туре	E_{AB} (Hartree)	E _A (Hartree)	$E_{\rm B}$ (Hartree)	$E_{\rm int}({\rm Hartree})$	E _{bind} (kcal/mol)
azido-azido	-407.906462	-203.952153	-203.952153	-0.002156	1.35
azido-carbamate	-527.485548	-203.952153	-323.527993	-0.005402	3.39
azido-urea	-507.619514	-203.952153	-303.659966	-0.007395	4.64
carbamate-carbamate	-647.067102	-323.527993	-323.527993	-0.011116	6.98
carbamate-urea	-627.201703	-323.527993	-303.659966	-0.013744	8.62
urea-urea	-607.336345	-303.659966	-303.659966	-0.016413	10.30
вно-вно	-833.936329	-416.948187	-416.948187	-0.039955	25.07
UPy-UPy	-1669.807886	-834.861765	-834.861765	-0.084356	52.93
HPS-HPS	-1488.220268	-744.093340	-744.093340	-0.033588	21.08

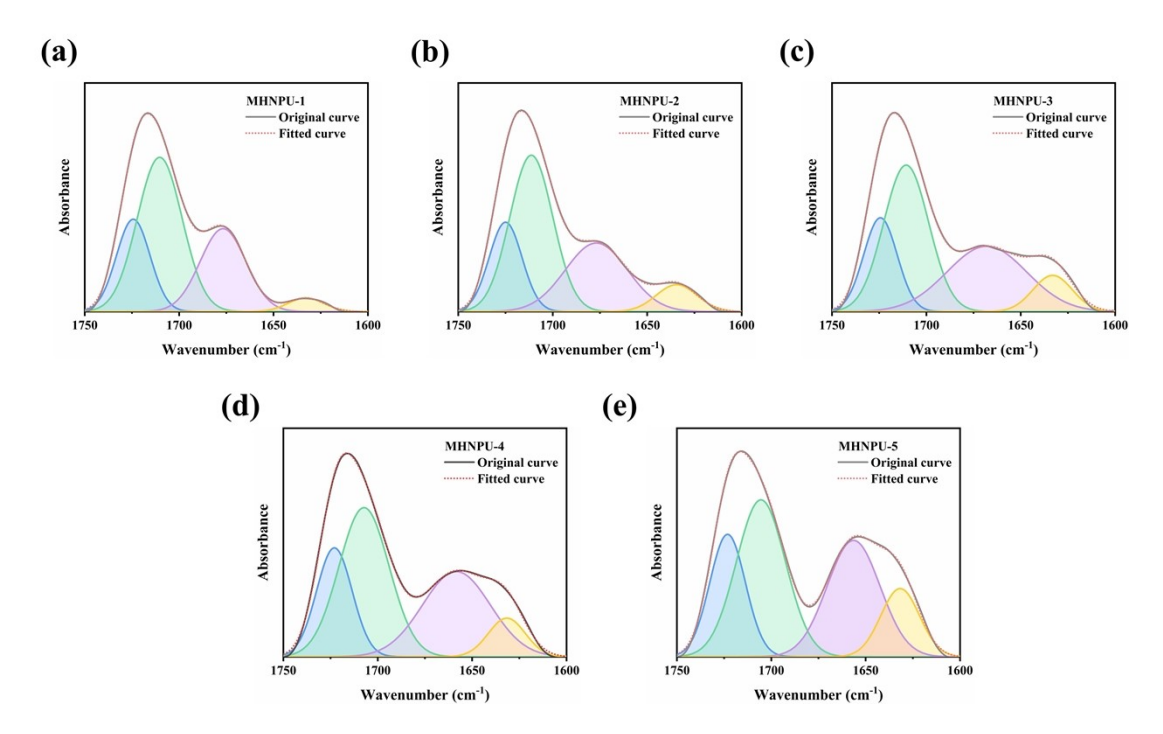


Figure 31 The peak splitting fitting curve of MHNPU-1-5 elastomers. The blue, green, purple, and yellow colors in the area correspond to the presence of free carbamate, H-bonded carbamate & free urea, disordered urea, and ordered urea, respectively.

Table S9 The FT-IR fitting results of MHNPU-1-5 elastomers.

Sample	Area I (%)	Area II (%)	Area III (%)	Area IV
Sample	Alca I (70)	Alca II (70)	Aica III (70)	(%)
MHNPU-1	21.68	48.32	26.55	3.43
MHNPU-2	19.51	44.70	28.47	7.31
MHNPU-3	19.16	40.34	31.83	8.67
MHNPU-4	20.81	40.25	31.23	7.71
MHNPU-5	20.89	36.91	29.58	12.62

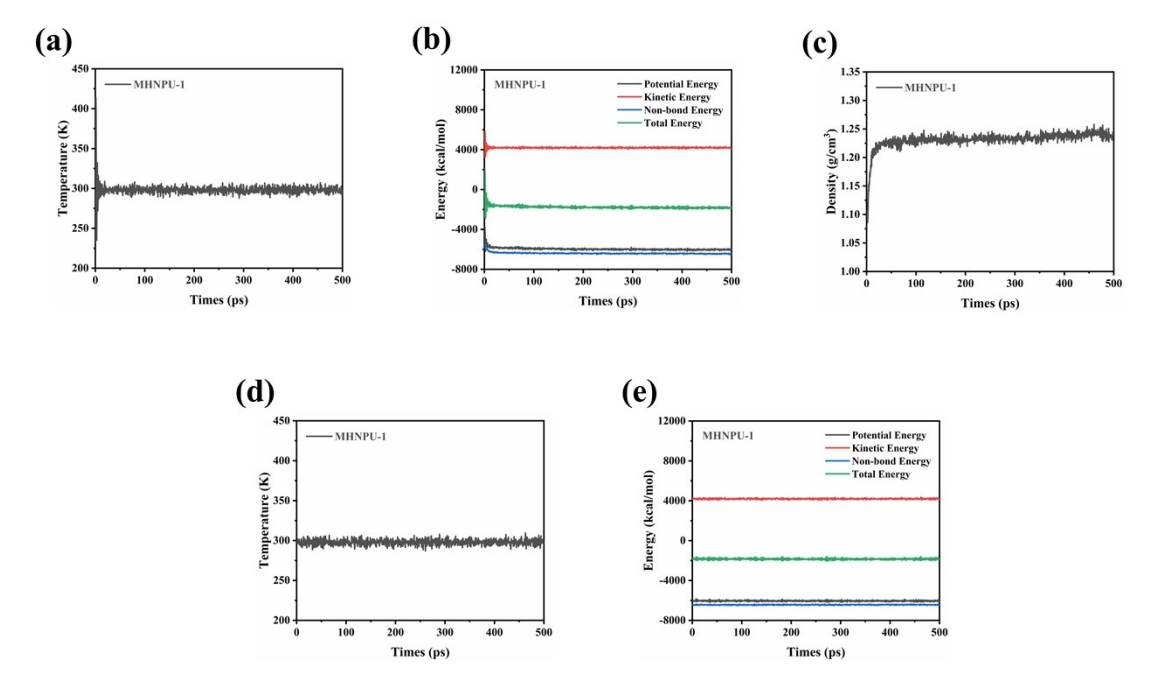


Figure S32 (a) Temperature vs. Times curves of MHNPU-1 with 500 ps NPT dynamics. (b) Energy (Potential, Kinetic, Non-bond, and Total Energy) vs. Times curves of MHNPU-1 with 500 ps NPT dynamics. (c) Density vs. Times curves of MHNPU-1 with 500 ps NPT dynamics. (d) Temperature vs. Times curves of MHNPU-1 with 500 ps NVT dynamics. (e) Energy (Potential, Kinetic, Non-bond, and Total Energy) vs. Times curves of MHNPU-1 with 500 ps NVT dynamics.

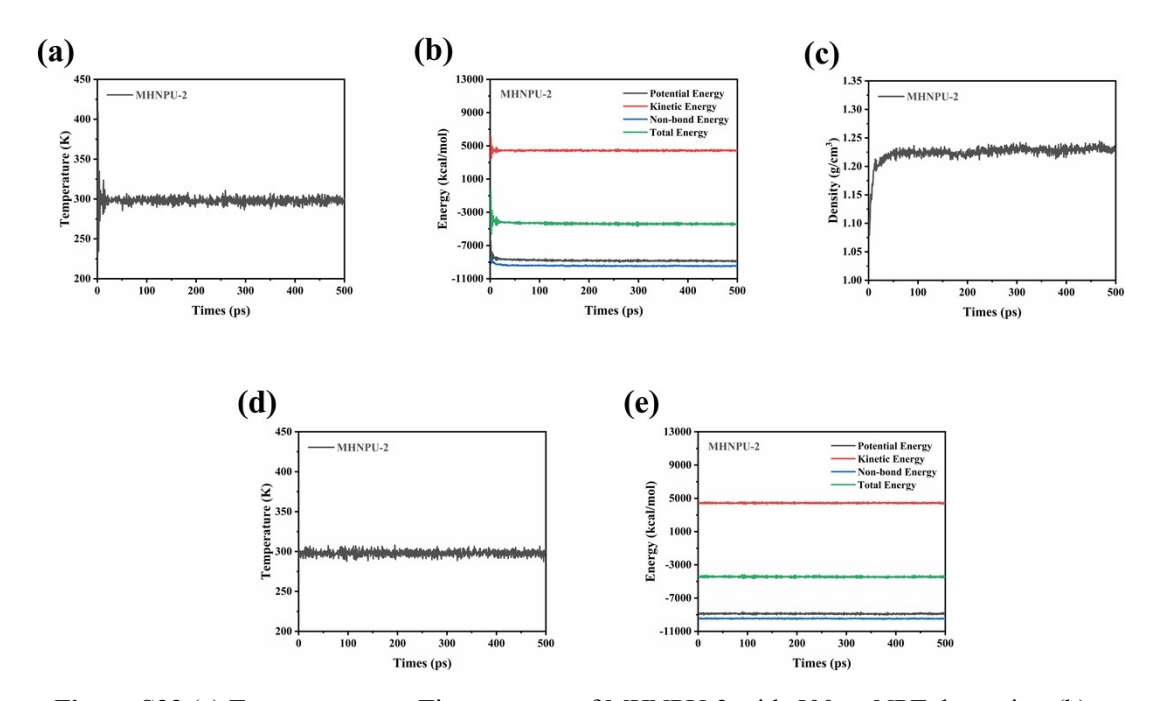


Figure S33 (a) Temperature vs. Times curves of MHNPU-2 with 500 ps NPT dynamics. (b) Energy (Potential, Kinetic, Non-bond, and Total Energy) vs. Times curves of MHNPU-2 with 500 ps NPT dynamics. (c) Density vs. Times curves of MHNPU-2 with 500 ps NPT dynamics. (d) Temperature vs. Times curves of MHNPU-2 with 500 ps NVT dynamics. (e) Energy (Potential, Kinetic, Non-bond, and Total Energy) vs. Times curves of MHNPU-2 with 500 ps NVT dynamics.

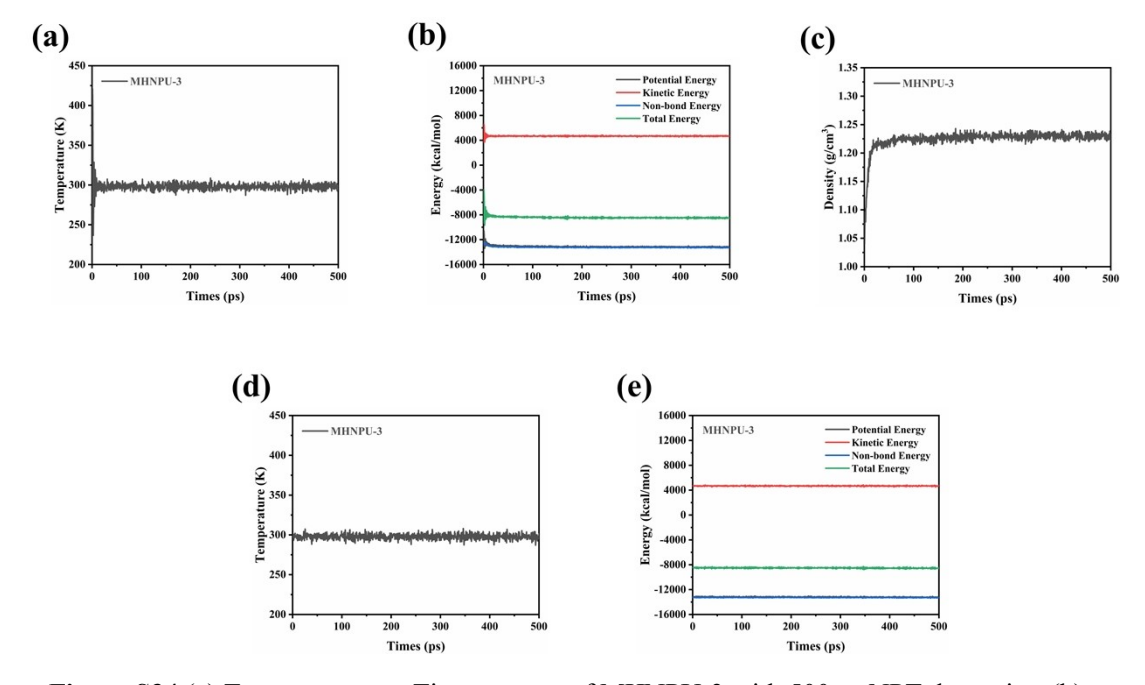


Figure S34 (a) Temperature vs. Times curves of MHNPU-3 with 500 ps NPT dynamics. (b) Energy (Potential, Kinetic, Non-bond, and Total Energy) vs. Times curves of MHNPU-3 with 500

ps NPT dynamics. (c) Density vs. Times curves of MHNPU-3 with 500 ps NPT dynamics. (d)
Temperature vs. Times curves of MHNPU-3 with 500 ps NVT dynamics. (e) Energy (Potential,
Kinetic, Non-bond, and Total Energy) vs. Times curves of MHNPU-3 with 500 ps NVT dynamics.

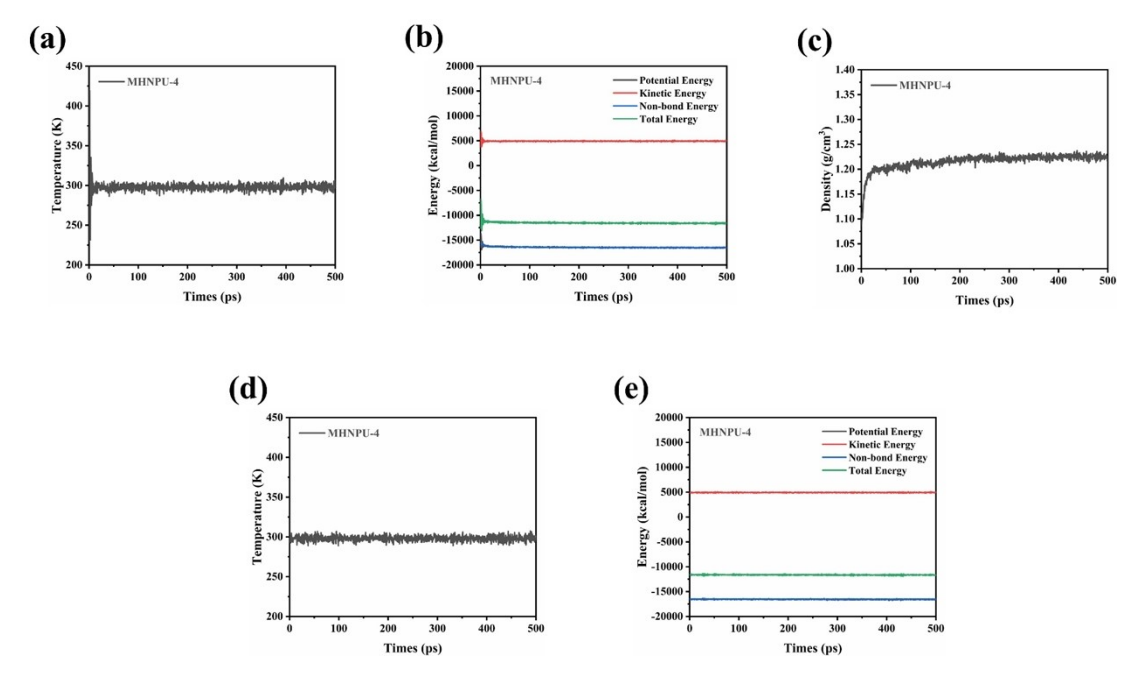


Figure S35 (a) Temperature vs. Times curves of MHNPU-4 with 500 ps NPT dynamics. (b) Energy (Potential, Kinetic, Non-bond, and Total Energy) vs. Times curves of MHNPU-4 with 500 ps NPT dynamics. (c) Density vs. Times curves of MHNPU-4 with 500 ps NPT dynamics. (d) Temperature vs. Times curves of MHNPU-4 with 500 ps NVT dynamics. (e) Energy (Potential, Kinetic, Non-bond, and Total Energy) vs. Times curves of MHNPU-4 with 500 ps NVT dynamics.

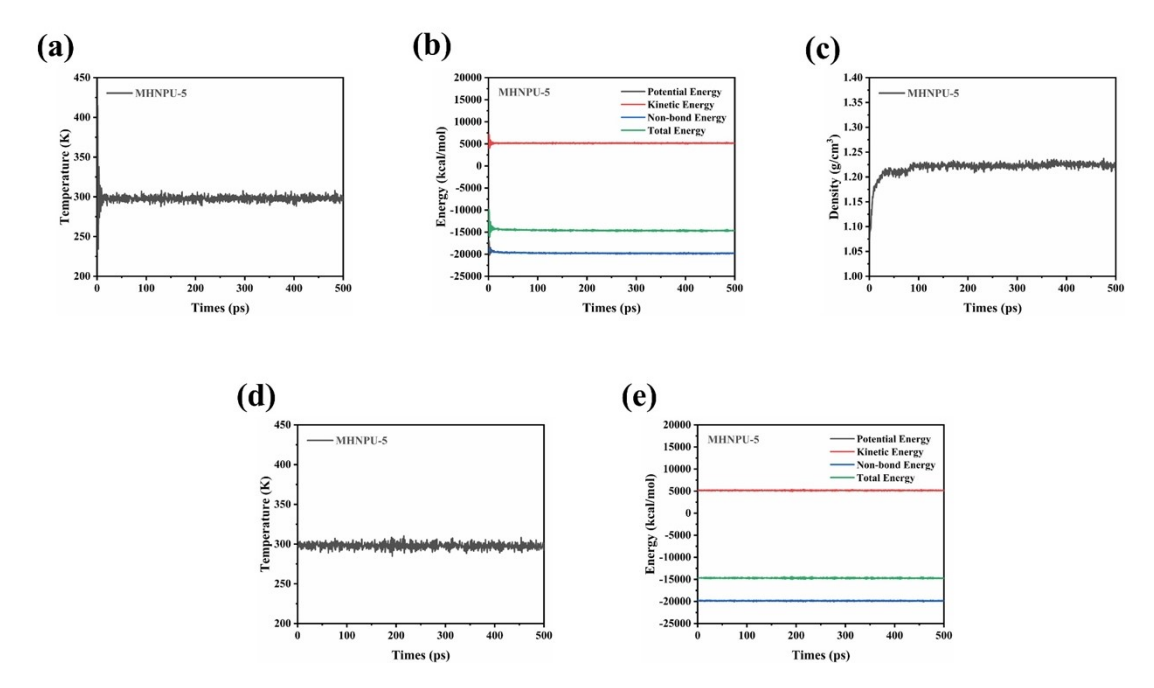


Figure S36 (a) Temperature vs. Times curves of MHNPU-5 with 500 ps NPT dynamics. (b) Energy (Potential, Kinetic, Non-bond, and Total Energy) vs. Times curves of MHNPU-5 with 500 ps NPT dynamics. (c) Density vs. Times curves of MHNPU-5 with 500 ps NPT dynamics. (d) Temperature vs. Times curves of MHNPU-5 with 500 ps NVT dynamics. (e) Energy (Potential, Kinetic, Non-bond, and Total Energy) vs. Times curves of MHNPU-5 with 500 ps NVT dynamics.

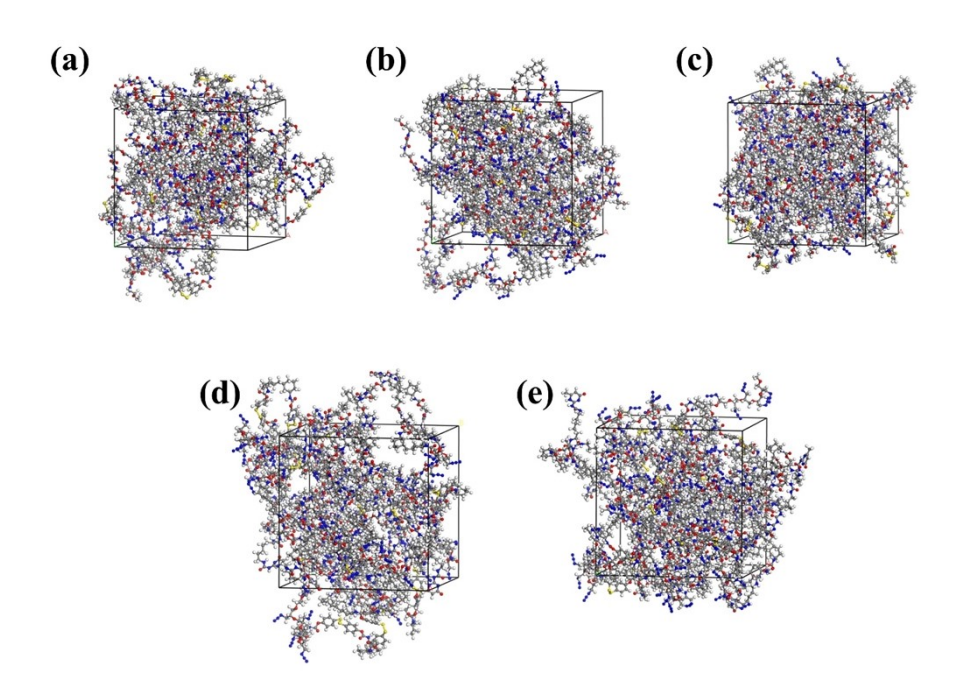


Figure S37 The equilibrium configuration of (a) MHNPU-1, (b) MHNPU-2, (c) MHNPU-3, (d) MHNPU-4, and (e) MHNPU-5 after dynamic simulation.

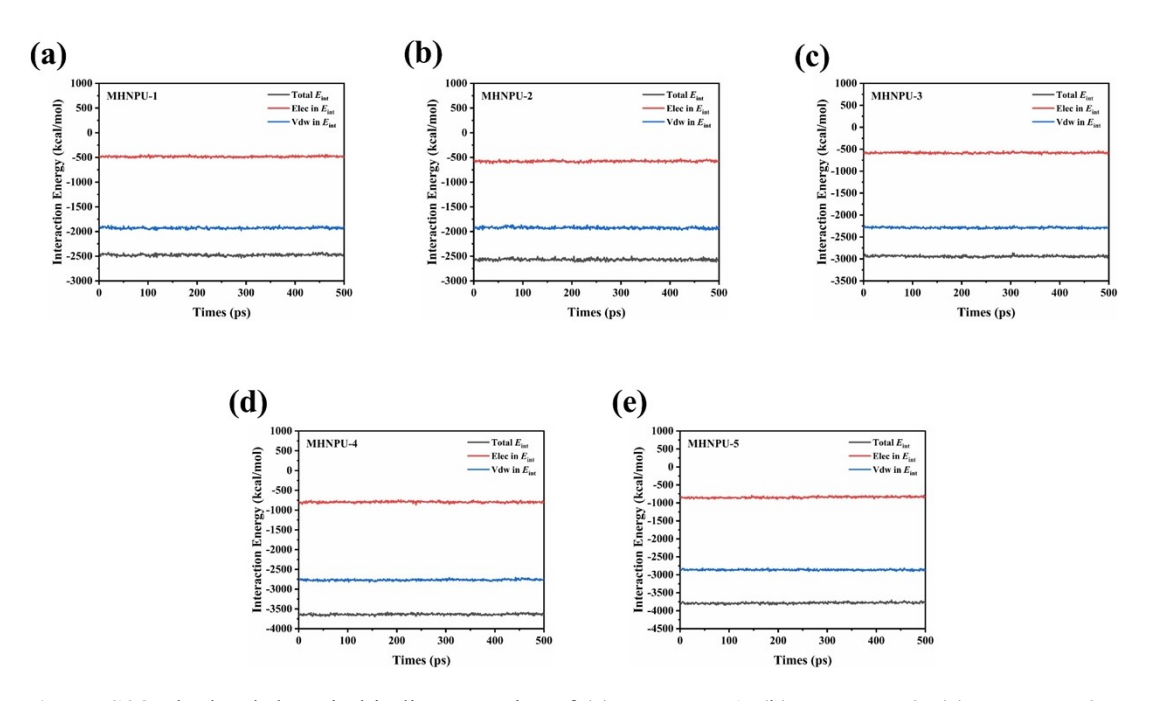


Figure S38 The hard-domain binding energies of (a) MHNPU-1, (b) MHNPU-2, (c) MHNPU-3, (d) MHNPU-4, and (e) MHNPU-5 during the 500 ps NVT dynamics.

Table S10 The summary of the number, length, and angle of H-bonds for MHNPU-1-5.

Sample	Number	Length (Å)	Angle (°)
MHNPU-1	286.63±8.41	2.65±0.49	127.38±23.76
MHNPU-2	327.54±8.24	2.64±0.49	129.58±24.28
MHNPU-3	352.63±9.37	2.67±0.51	132.41±23.07
MHNPU-4	401.26±9.74	2.67±0.59	132.74±22.24
MHNPU-5	411.32±10.0 8	2.70±0.59	134.79±21.09

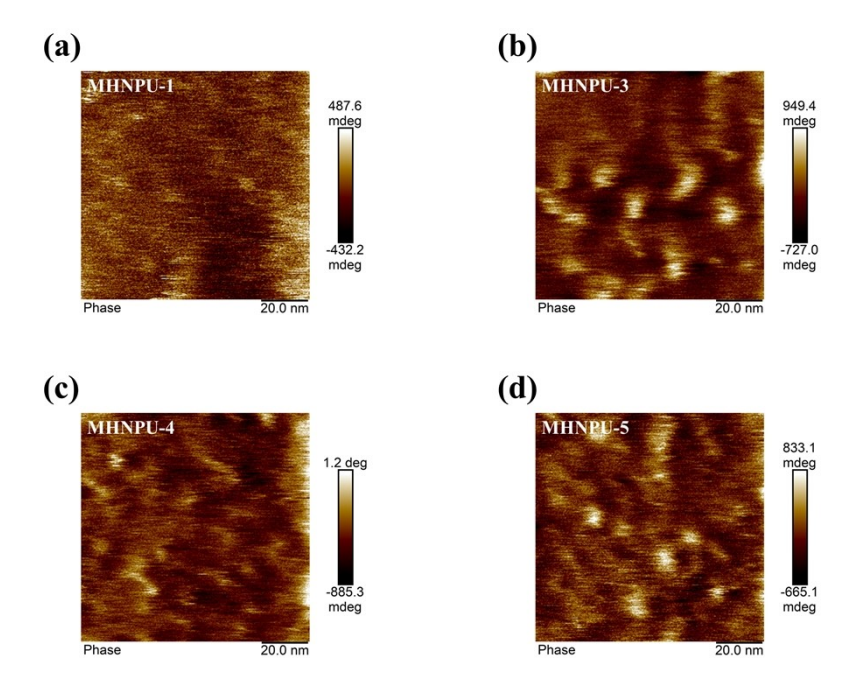


Figure S39 The atomic force microscopy (AFM) phsase images of (a) MHNPU-1, (b) MHNPU-3, (c) MHNPU-4, and (d) MHNPU-5 with tapping mode.

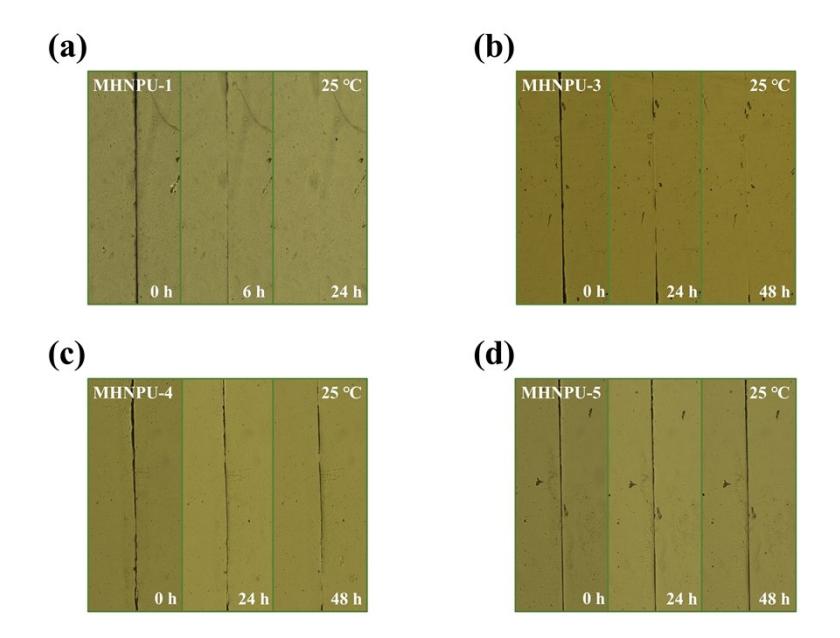


Figure S40 Optical microscopy of the self-healing process of (a) MHNPU-1, (b) MHNPU-3, (c) MHNPU-4, and (d) MHNPU-5 polymerss at room temperature for different healing times.

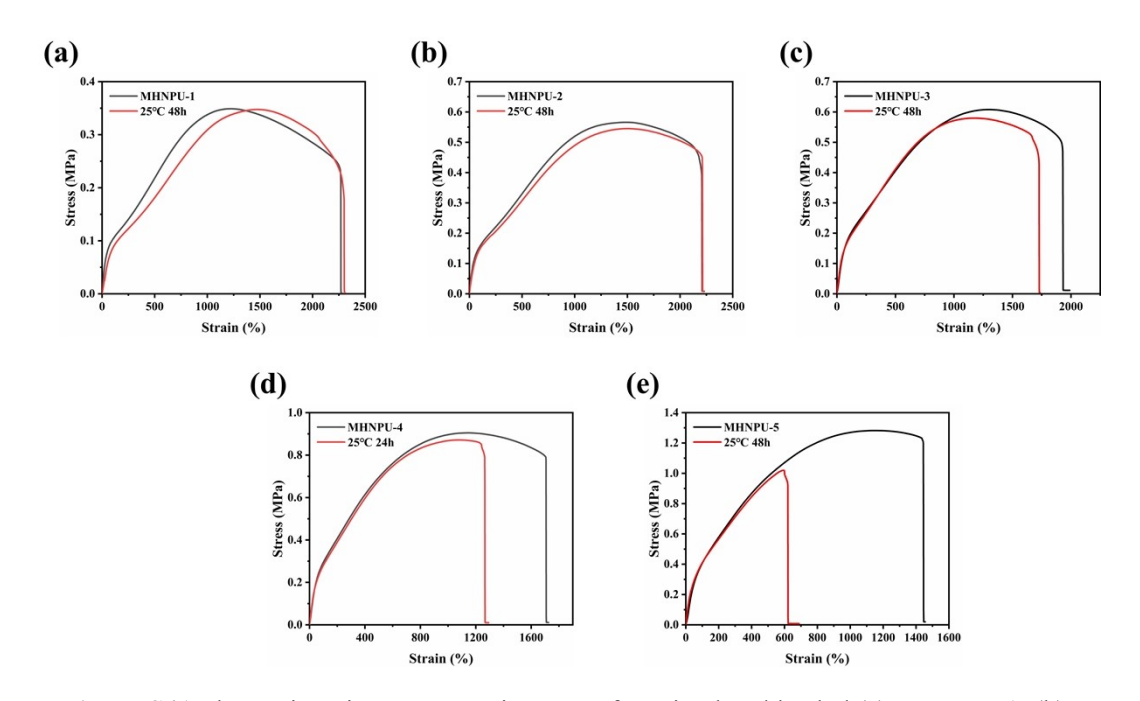


Figure S41 The engineering stress-strain curves for primal and healed (a) MHNPU-1, (b) MHNPU-2, (c) MHNPU-3, (d) MHNPU-4, and (e) MHNPU-5 polymers at room temperature.

Table S11 The mechanical properties of healed MHNPU-1-5 elastomers under different healing time.

Sample	Healing Temperature	Healing Time	Stress (MPa)	Strain (%)	Toughness (MJ/m ³)
MHNPU-1	25 °C	48 h	0.35±0.09	2301±77	5.96±0.35
MHNPU-2	25 °C	1 h	0.37±0.03	609±34	1.38±0.06
MHNPU-2	25 °C	6 h	0.51±0.07	1098±47	3.75±0.15
MHNPU-2	25 °C	12 h	0.56±0.06	1743±43	7.36±0.17
MHNPU-2	25 °C	24 h	0.55±0.08	2027±65	8.61±0.33
MHNPU-2	25 °C	48 h	0.55±0.09	2214±81	9.36±0.48
MHNPU-3	25 °C	48 h	0.58±0.07	1729±94	7.92±0.61
MHNPU-4	25 °C	48 h	0.87±0.13	1267±73	8.45±0.47
MHNPU-5	25 °C	48 h	1.01±0.15	621±51	4.27±0.53

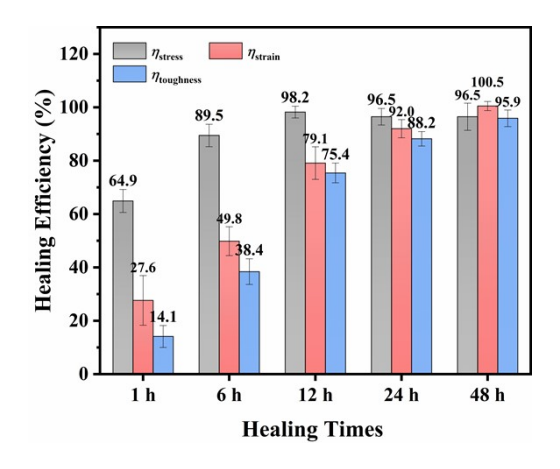


Figure S42 The healing efficiency of MHNPU-2 with a temperature of 25 °C for different healing time.

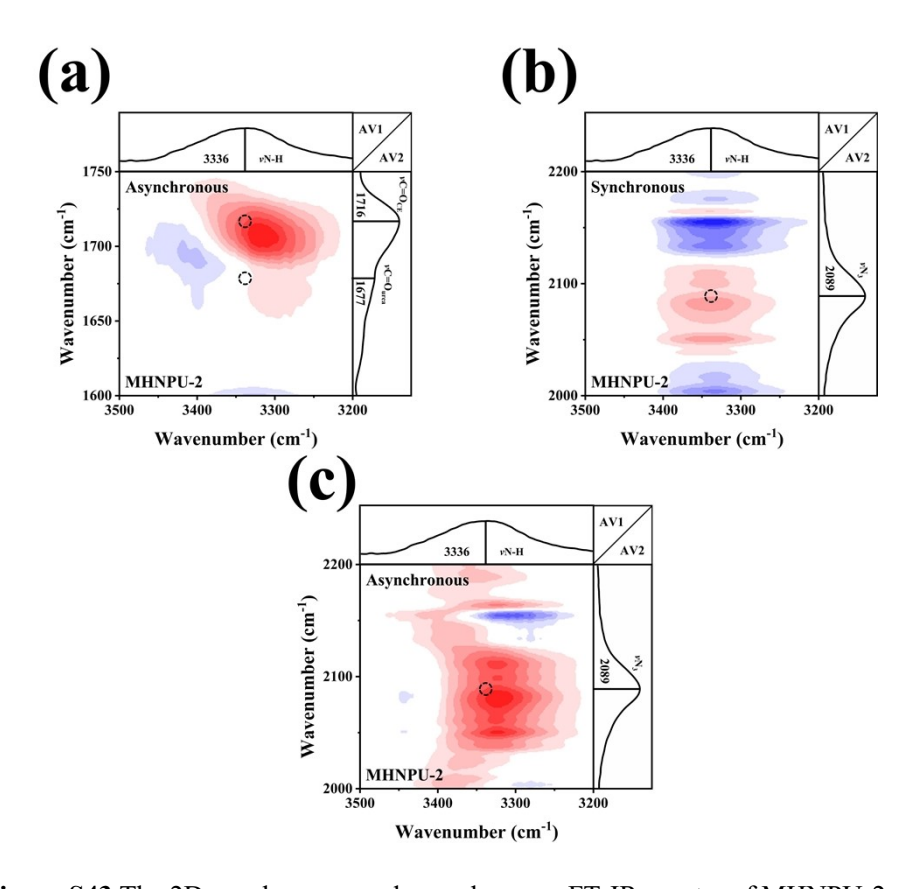


Figure S43 The 2D synchronous and asynchronous FT-IR spectra of MHNPU-2.

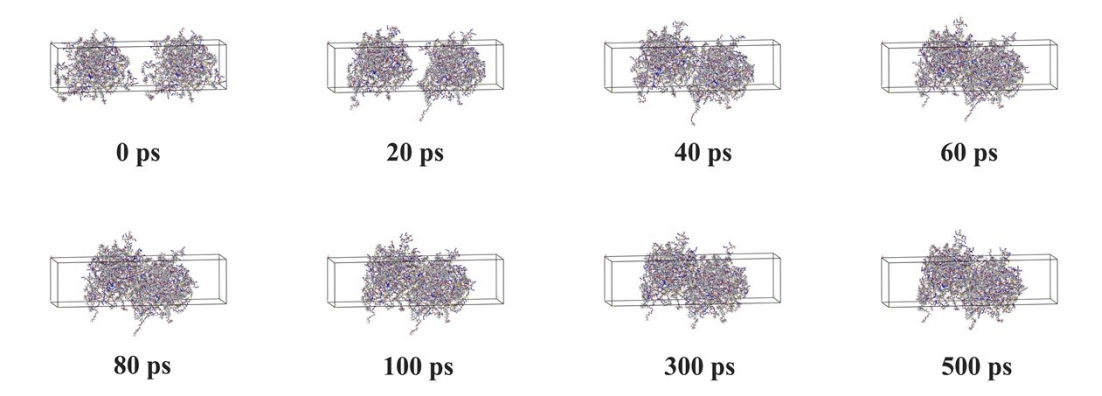


Figure S44 The trajectory of the MHNPU-2 crack model over a 500 ps run using the NVT ensemble at 298 K.

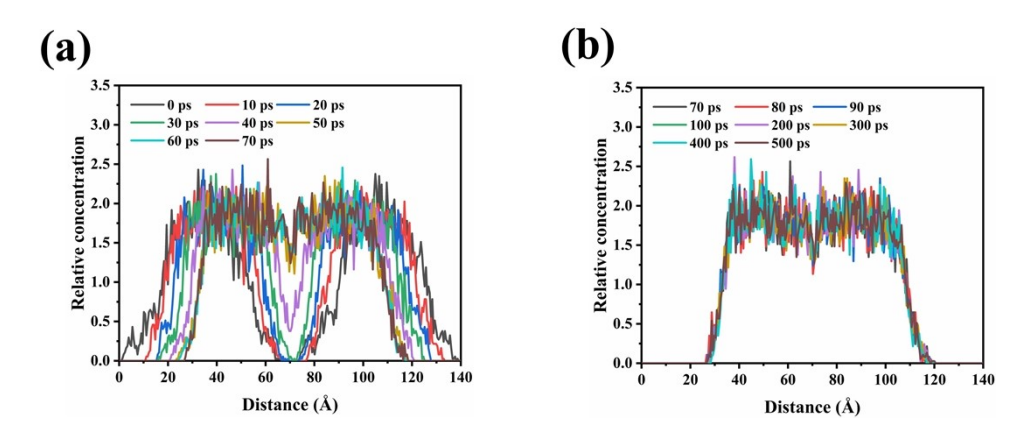


Figure S45 The concentration profiles of MHNPU-2 crack model in the range of (a) 0-70 ps and (b) 70-500 ps at a temperature of 298 K.

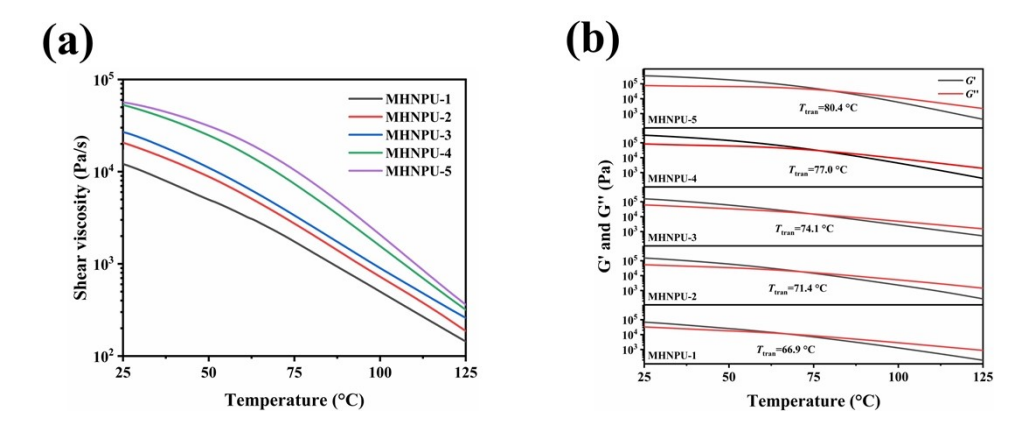


Figure S46 (a) The shear viscosity vs. temperature curves and (b) The modulus vs. temperature curves of MHNPU-1-5 with a shear strain of 1 % and a frequency of 1 Hz.

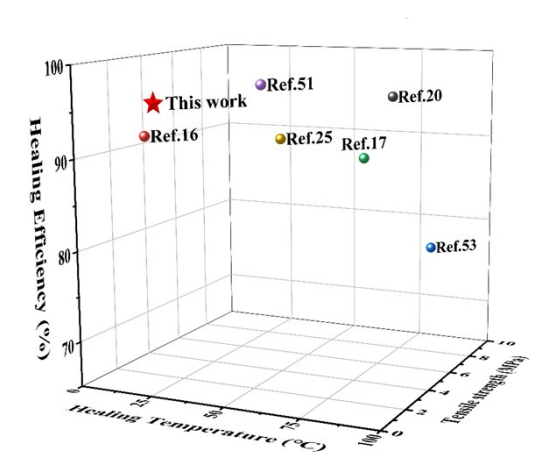


Figure S47 A comparison between the mechanical and healing properties from this work and previously reported energetic self-healing polymers from the literature

Table S12 A comparison of the mechanical and healing properties of MHNPU-2 polymer with those of other reported energetic self-healing polymers.

Sample	Tensile strength (MPa)	Healing Temperature (°C)	Healing Efficiency (%)	Ref.
GAPUVs (P40- 90)	4.70	85	96.2	20
GAP-IDI-MDA	0.03	25	92.9	16
GAP EPU5	6.89	90	78.4	53
GAP-H ₄ I ₆ - IPDH	3.61	80	90.0	17
GSPU2.5	0.72	60	98.4	51
AAE-3	1.98	60	92.4	25
MHNPU-2	0.57	25	96.1	This work

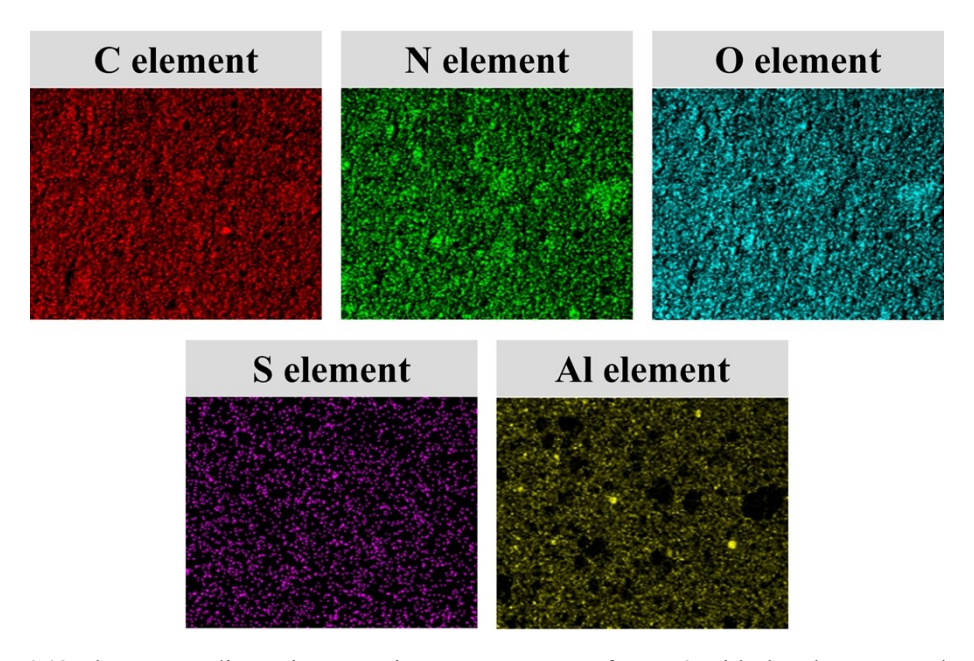


Figure S48 The energy dispersive mapping spectroscopy of DSP-2 with the elements carbon (C), nitrogen (N), oxygen (O), sulfur (S), and aluminum (Al).

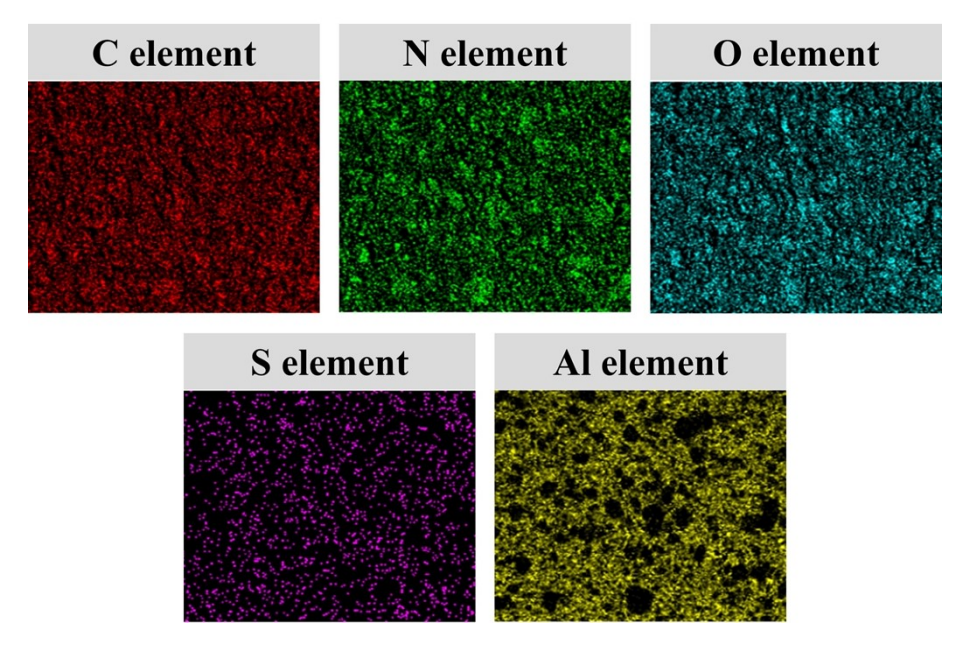


Figure S49 The energy dispersive mapping spectroscopy of DSP-3 with the elements carbon (C), nitrogen (N), oxygen (O), sulfur (S), and aluminum (Al).

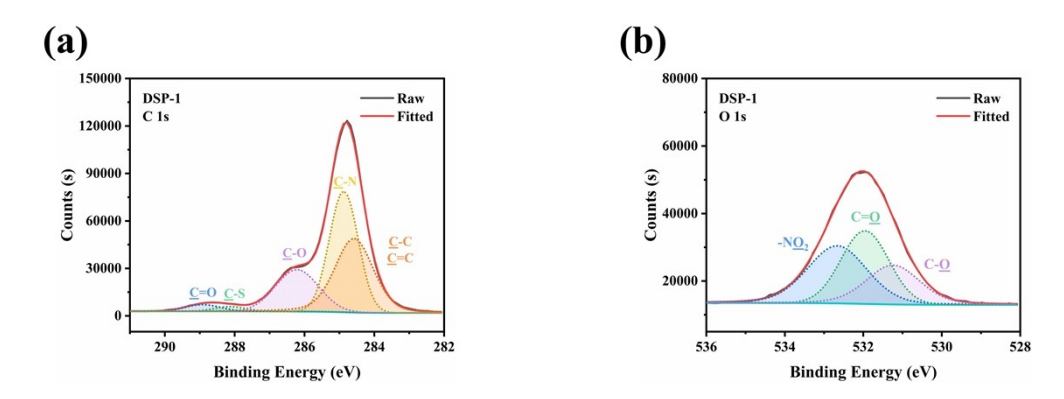


Figure S50 High-resolution XPS spectra of (a) C 1s and (b) O 1s regions for DSP-1.

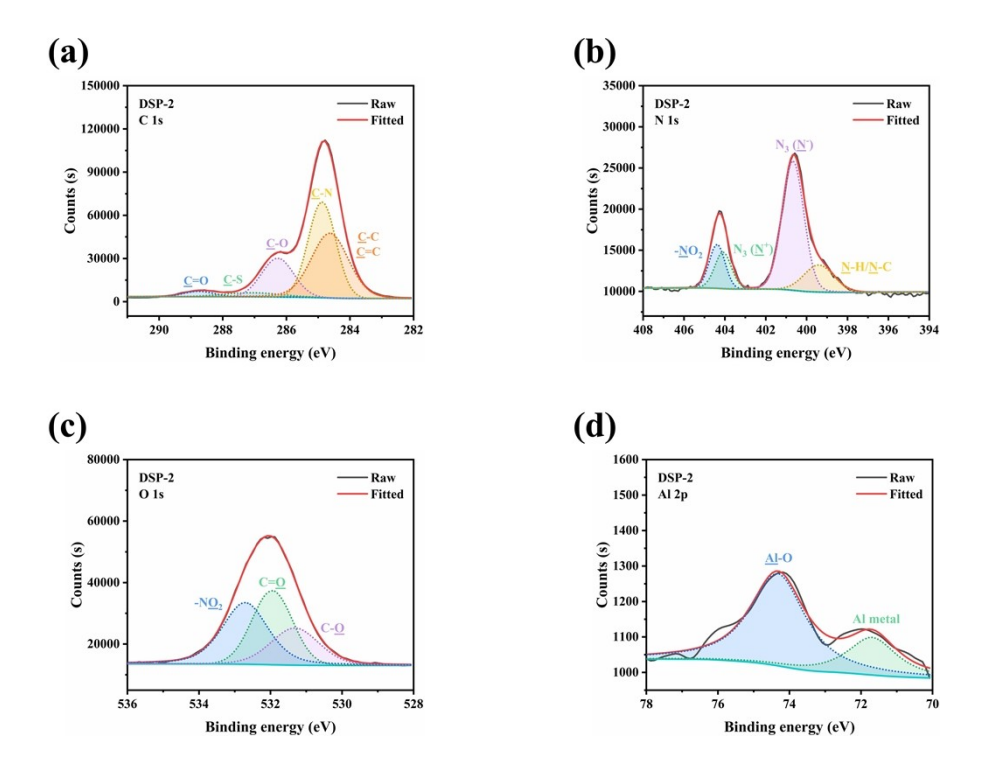


Figure S51 High-resolution XPS spectra of (a) C 1s, (b) N 1s, (c) O 1s, and (d) Al 2p regions for DSP-2.

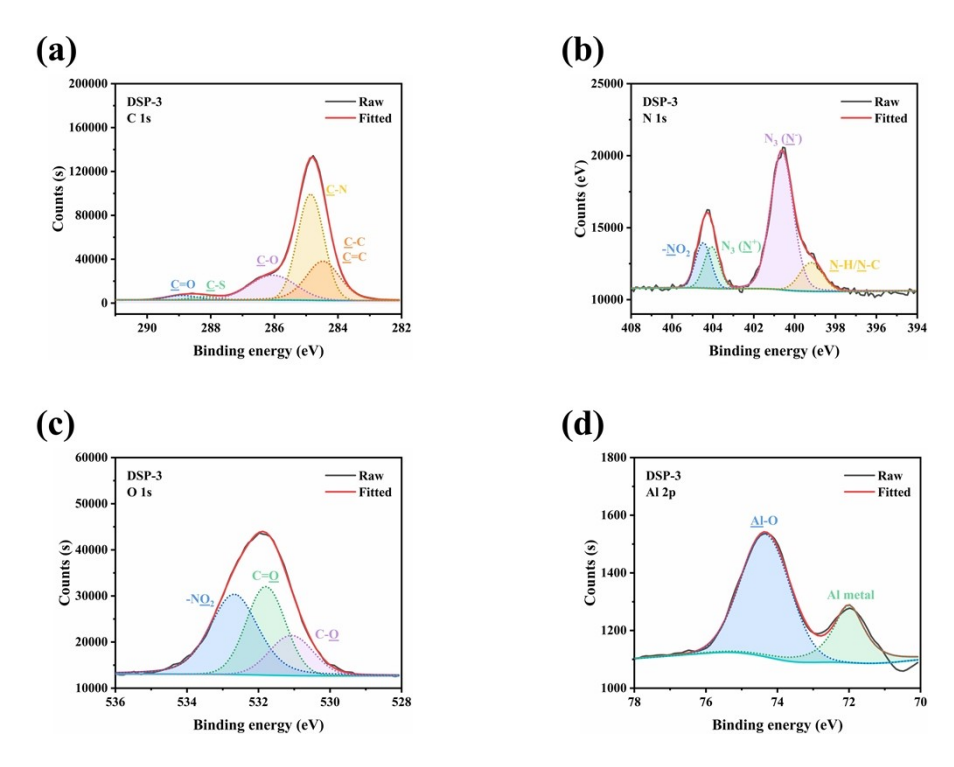


Figure S52 High-resolution XPS spectra of (a) C 1s, (b) N 1s, (c) O 1s, and (d) Al 2p regions for DSP-3.

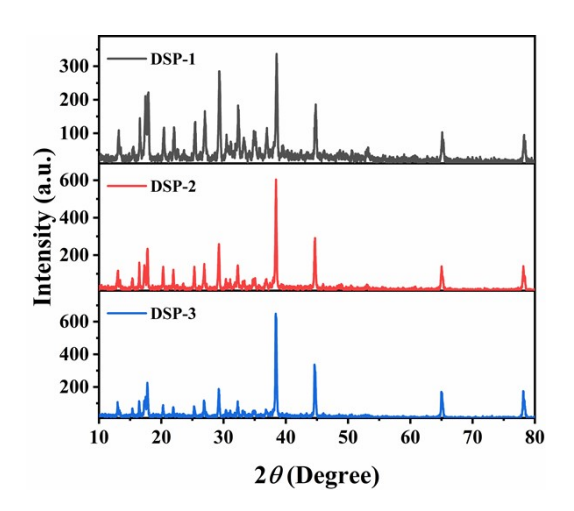


Figure S53 The XRD data of DSP-1-3 with a scanning speed of 5 degree/min.

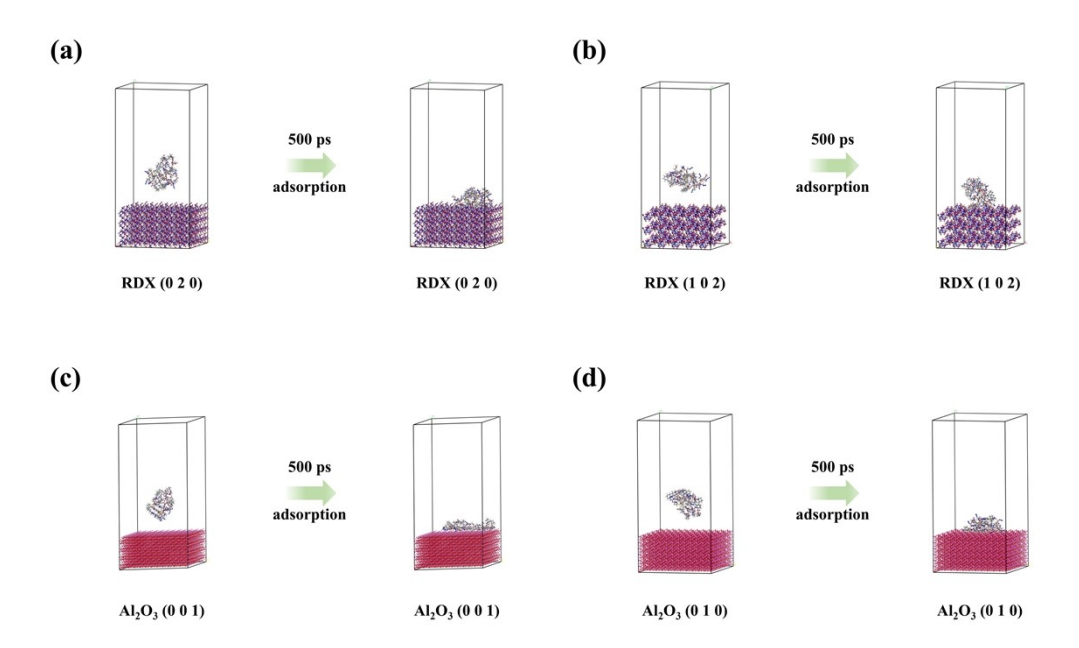


Figure S54 The adsorption process between MHNPU-2 polymer and (a) RDX (0 2 0) crystal plane, (b) RDX (1 0 2) crystal plane, (c) Al_2O_3 (0 0 1) crystal plane, and (d) Al_2O_3 (0 1 0) crystal plane.

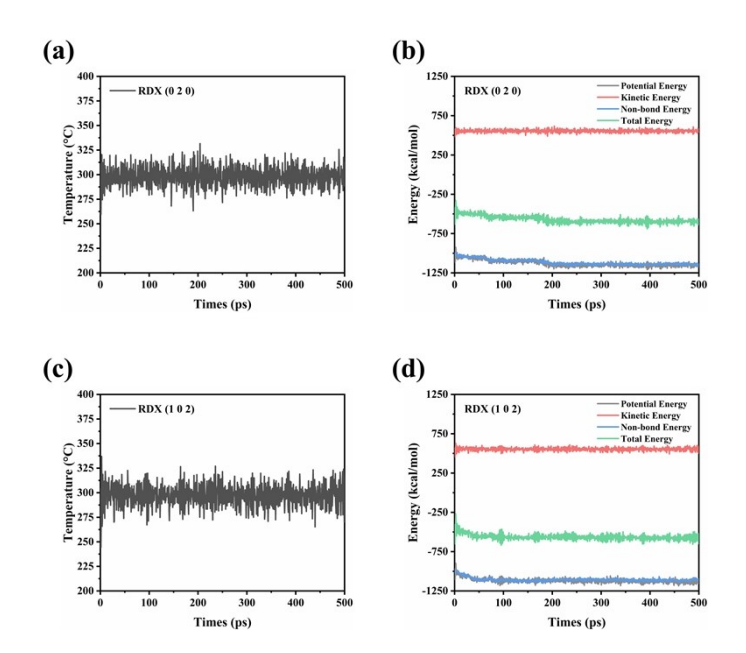


Figure S55 (a) Temperature vs. Times curves of RDX (0 2 0) with 500 ps NVT dynamics. (b)

Energy (Potential, Kinetic, Non-bond, and Total Energy) vs. Times curves of RDX (0 2 0) with

500 ps NVT dynamics. (c) Temperature vs. Times curves of RDX (1 0 2) with 500 ps NVT

dynamics.. (d) Energy (Potential, Kinetic, Non-bond, and Total Energy) vs. Times curves of RDX

(1 0 2) with 500 ps NVT dynamics.

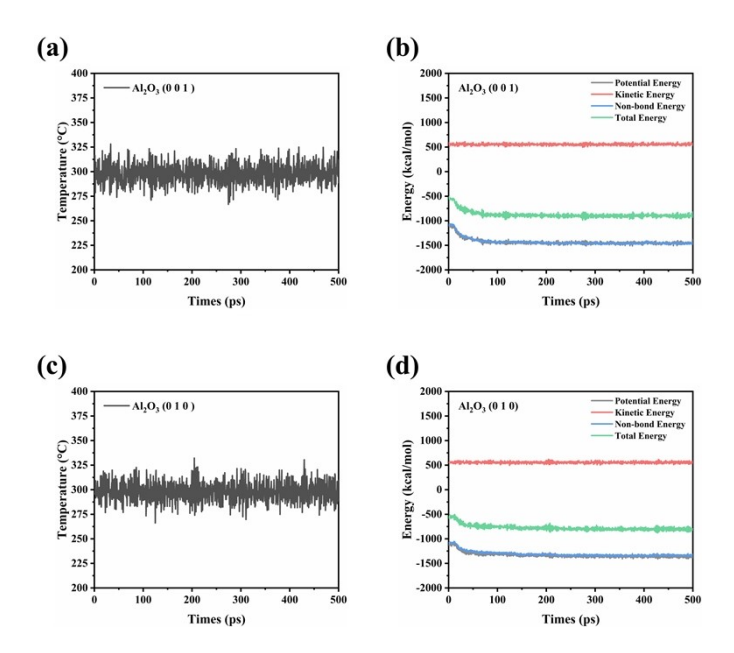


Figure S56 (a) Temperature vs. Times curves of Al₂O₃ (0 0 1) with 500 ps NVT dynamics. (b)

Energy (Potential, Kinetic, Non-bond, and Total Energy) vs. Times curves of Al₂O₃ (0 0 1) with

500 ps NVT dynamics. (c) Temperature vs. Times curves of Al₂O₃ (0 1 0) with 500 ps NVT

dynamics.. (d) Energy (Potential, Kinetic, Non-bond, and Total Energy) vs. Times curves of Al₂O₃

(0 1 0) with 500 ps NVT dynamics.

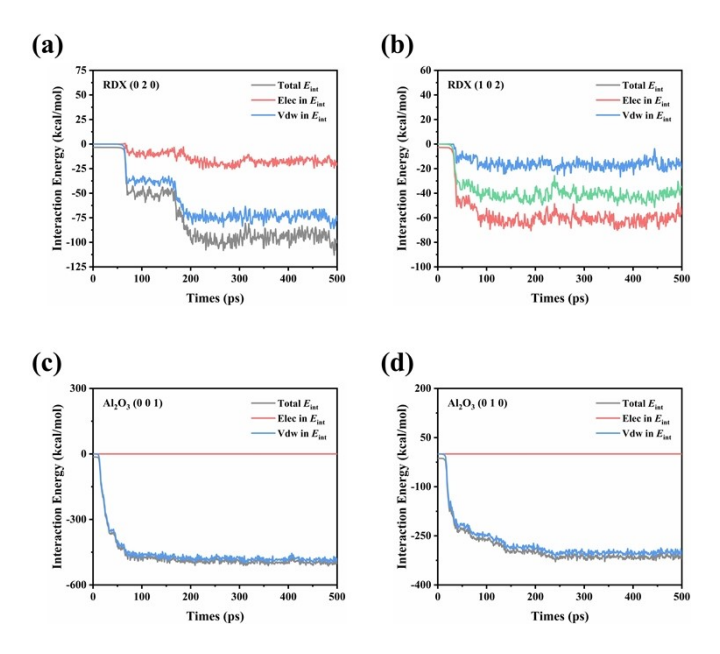


Figure S57 Energy contribution (Total, elec., vdW.) to interfacial interaction energy for adsorption model between polymer and (a) RDX (0 2 0) crystal plane, (b) RDX (1 0 2) crystal plane, (c) Al₂O₃ (0 0 1) crystal plane, and (d) Al₂O₃ (0 1 0) crystal plane.

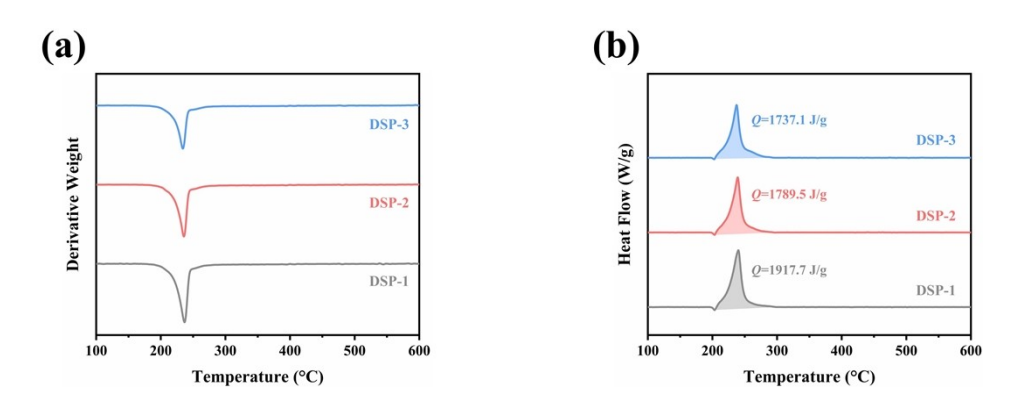


Figure S58 (a) Derivative weight curves of DSP-1-3 with a heating rate of 10 K/min, and (b) differential scanning calorimetry curves of DSP-1-3 with a heating rate of 10 K/min (The upward peak is the exothermic process).

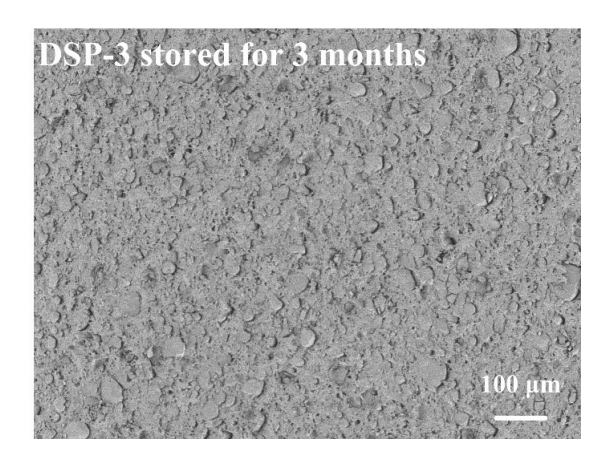


Figure S59 The cross-sectional scanning electronic microscopy of DSP-3 stored for 3 months.

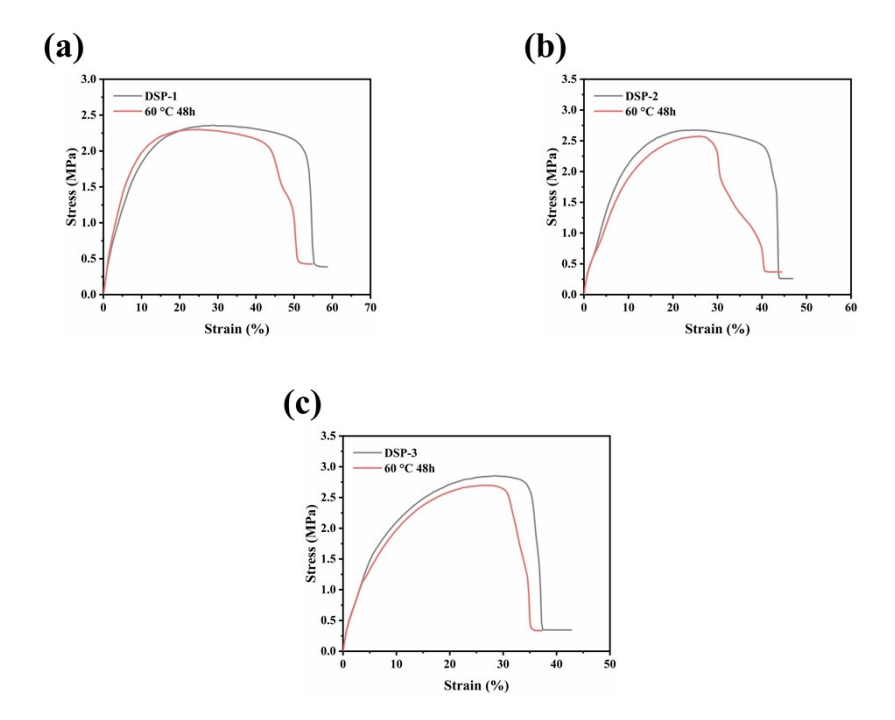


Figure S60 The engineering stress-strain curves of healed and intact (a) DSP-1, (b) DSP-2, and (c) DSP-3.

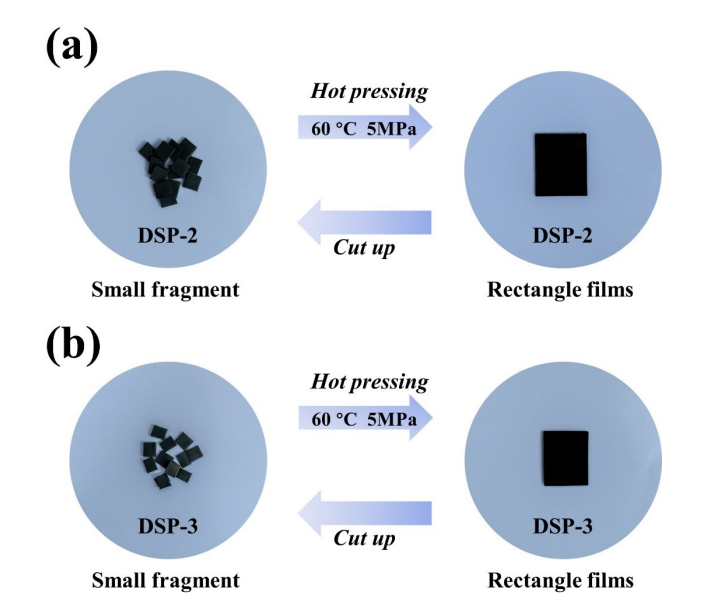


Figure S61 The picture of hot-pressing process for (a) DSP-1, (b) DSP-2, and (c) DSP-3.

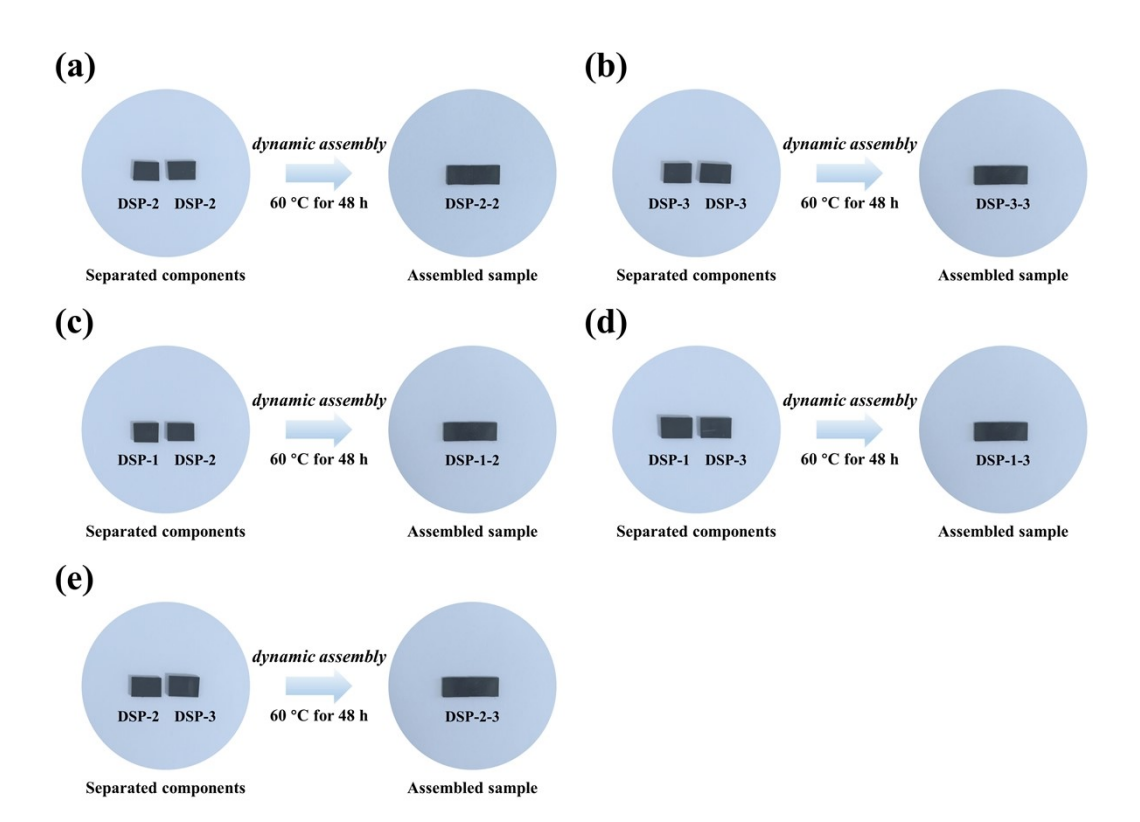


Figure S62 Schematic diagram of the dynamic assembly process of (a) DSP-2-2; (b) DSP-3-3; (c) DSP-1-2; (d) DSP-1-3; (e) .DSP-2-3.

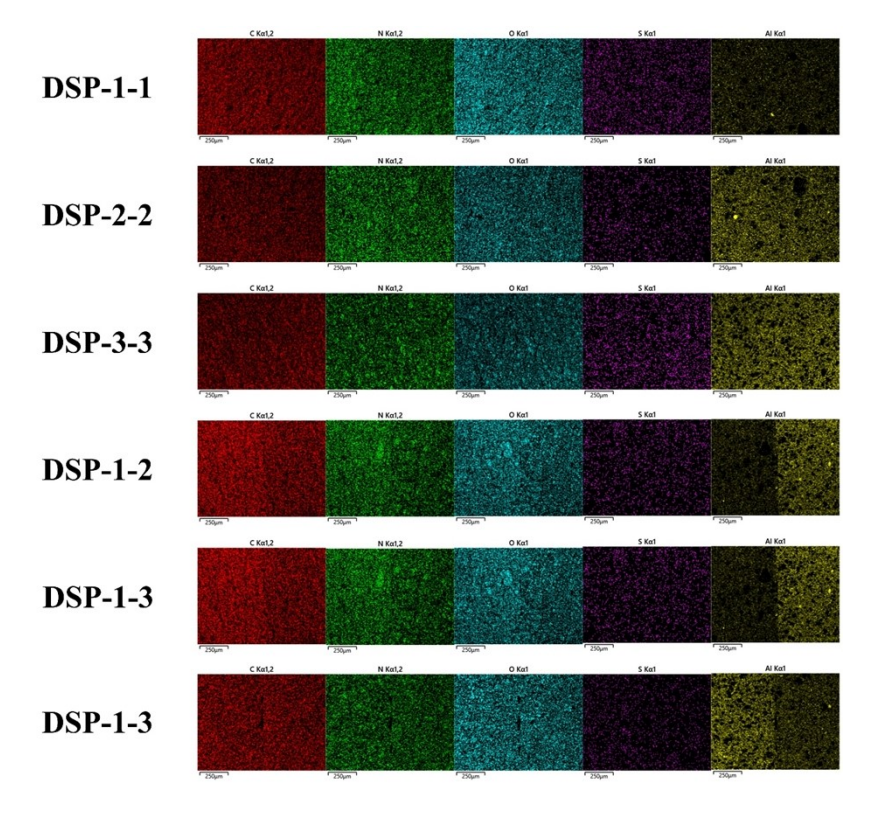


Figure S63 The energy dispersive mapping spectroscopy of DSP-1-1, DSP-2-2, DSP-3-3, DSP-1-

2, DSP-1-3, and DSP-2-3 with the elements carbon (C), nitrogen (N), oxygen (O), sulfur (S), and aluminum (Al).

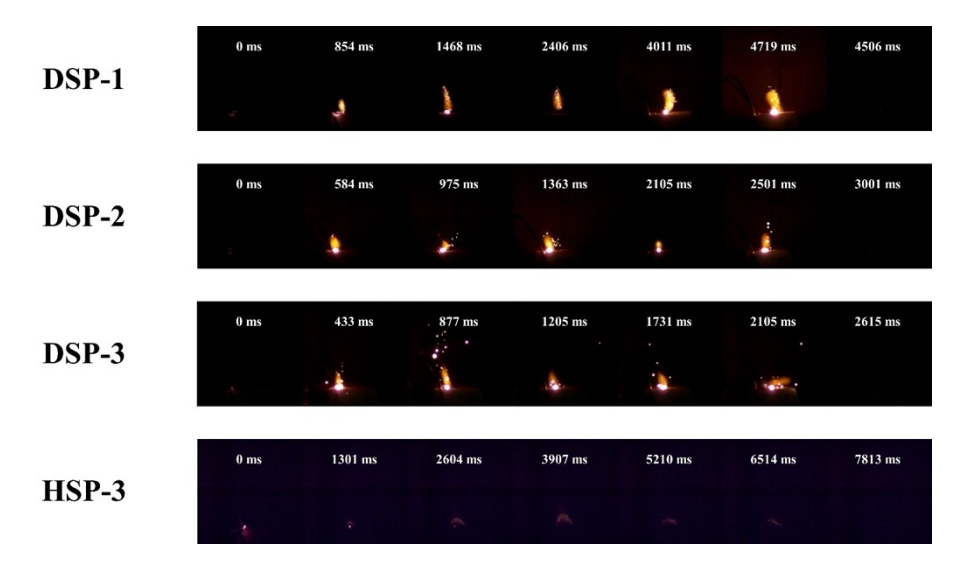


Figure S64 The open combustion experiments of DSP-1, DSP-2, DSP-3, and HSP-3. HSP-3 was developed with a hydroxyl-terminated polybutadiene binder, with RDX and Al concentration equivalent to those of DSP-3 (The length of the samples tested were 15 mm.).